Genetic resolution of dopamine systems for reward association and motivation

Gabriel Heymann

A dissertation

submitted in partial fulfillment of the

requirements for the degree of

Doctor of Philosophy

University of Washington

2018

Reading Committee

Larry Zweifel, Chair

Paul Phillips, Ph.D.

Richard Palmiter, Ph.D.

Program Authorized to Offer Degree:

Molecular and Cellular Biology program

University of Washington

Abstract

Genetic resolution of dopamine systems for reward association and motivation

Gabriel Heymann

Chair of Supervisory Committee:

Larry S. Zweifel

Departments of Pharmacology and Psychiatry

The ventral tegmental area (VTA) dopamine system is a key regulator of reward and motivational processes[1-3]. Through modulation of cortico- and amygdalo-striatal networks, VTA dopamine neurons facilitate and update stimulus- and response-outcome associations[4-9]. They also provide a motivational signal that initiates and sustains approach behavior in response to reward-predictive stimuli[1,10,11]. It has been proposed that these two components of reward behavior represent discrete dopamine systems, but the populations and pathways that comprise them remain unresolved. Based on gene enrichment data in midbrain dopamine neurons, we utilized neuropeptidergic markers to genetically isolate VTA dopamine subpopulations. Characterization revealed two primarily distinct

subpopulations with unique projection patterns to mesolimbic targets, including the core and shell subdivisions of the nucleus accumbens (NAc). *In vivo* electrophysiological analysis during an instrumental reward paradigm demonstrated similar phasic responses to reward-related actions and stimuli, and a tonic rise in baseline firing preceding reward receipt during early learning. However, these responses diverged as training progressed indicating differential adaptations with extended conditioning. Optogenetic manipulation of these populations revealed dissociable roles in the formation of reward associations or the maintenance of learned reward behaviors, and that convergence of these associative and motivational systems is required to maximize reward reinforcement. Our findings begin to consolidate the operational roles of discrete dopamine populations and pathways, a crucial step in identifying more precise therapeutic targets for drug addiction and depression, disorders associated with aberrations in mesolimbic dopamine signaling[12-15].

Acknowledgments

There have been so many people that have helped and supported me, both personally and professionally over the course of my training. To the past and current members of the Zweifel lab, thank you for your continued guidance and for making this a powerful learning experience in so many ways. To Larry, I thank you for being an always-present mentor, while providing independence and encouraging self-directed thought. I have enjoyed learning from you. My thesis committee has served as an important source of advice, making considerable contributions to my training and confidence as a scientist. I am forever grateful to have genuine advocates such as Fred, Bill, Paul and Richard.

To all of my friends, in Seattle and elsewhere, I am indebted to you. There are too many things to say thank you for. And most importantly, to my parents, sisters and other family, I am beyond thankful for your unwavering love and support.

Introduction

Dr. Arvid Carlsson first discovered the role of dopamine as a neurotransmitter in 1957[16]. Since then, extensive research has identified dopamine as a key modulator of network activity that regulates a diverse spectrum of cognitions, affective states and behaviors[2,10,17]. In accordance with this broad role in adaptive behavior, aberrant dopamine signaling has been implicated in an array of neuropsychiatric disorders and mental illness symptomology[12,13,18,19]. Elucidating the dopamine sub-systems underlying specific adaptive and disease processes has been a challenging, critical and ongoing pursuit.

Dopamine reward signals

Dopamine neurons encode reward-related information through dynamic changes in activity[2]. Transient, ~300-ms firing rate increases termed 'phasic' were first observed to receipt of unexpected reward and can emerge in response to reward-predictive stimuli once an association is formed[2]. Phasic firing has also been shown to signal the importance or salience of a stimulus, regardless of valence[20]. While these phasic signals encode discrete events, tonic firing rate is thought to set a baseline for behavioral activation that can progressively increase in pursuit of reward[21-23]. The precise role of these signals in reward learning and motivation is still under debate. Furthermore, little is known about how response heterogeneity segregates based on target site or molecular characteristics[20].

VTA mesolimbic reward pathways

The VTA is the origin of several dopaminergic circuits that project to diverse forebrain, cortical and subcortical structures. Among dopamine-receptive brain regions, the NAc is most broadly associated with reward processing[24-26]. Dopamine signaling in this region is thought to modulate synaptic strength in a context- and stimulus-specific manner to drive learning and expression of reward-related behaviors[4-7]. Extensive research has focused on how NAc subdivisions, the core and shell, differently contribute to discrete and/or interdependent reward processes. Considerable evidence points to a model in which the core plays a prominent role in prediction-error computations[27] and incentive-salience attribution[1], while the shell is thought to encode the current value of outcomes, suppress irrelevant action and motivate reward seeking and consumption behaviors[24,26]. This working model, however, is constrained by the limitations of current techniques. Combined optogenetic and intersectional strategies using retrograde virus delivery allow precise control of isolated circuit components[28,29], but may not target a sufficiently large population of cells to mediate an effect. Other approaches lack the temporal specificity necessary to manipulate dopamine dynamics on the timescales observed during behavior[11,24], or have been correlational in nature[25], precluding direct testing of causal relationships between circuit activity and behavioral outputs. All methodologies are further complicated by the spatial proximity of the core and shell subdivisions.

VTA heterogeneity

While the majority of neurons in the VTA are dopaminergic (~65-70%), there are also GABAergic (~30%) and glutamatergic subpopulations (~5%)[30]. Canonical dopamine neurons have also been shown to co-release glutamate[31,32], and recent studies have revealed important roles for VTA GABA[33,34] and glutamate[35,36] signaling in reward and aversion processing, adding to the cellular and circuit complexity of this system.

Genetic dissection of the VTA dopamine system

The spectrum of mental-illness symptomology linked to dopamine system dysfunction reflects its important role in adaptive behavior and highlights the need to further understand the organizational principles underlying its functional heterogeneity. Advances in circuit mapping and intersectional viral strategies have provided a framework in which subsets of dopamine neurons receive specific inputs, project to different target sites and have distinct electrophysiological, anatomical and molecular properties[30,37-40]. However, an inability to sufficiently manipulate dopamine neuron populations and pathways has precluded a rational segregation of functional sub-systems. Using a cell-type specific technique[41] to quantify actively translated mRNAs in VTA dopamine neurons, we identified a subset of neuropeptide receptors and the neuropeptide cholescyctokinin (*Cck*) with enriched expression in VTA dopamine neurons[42]. Based on this observation, in conjunction with several studies illustrating how neuropeptides modulate VTA dopamine neuron activity[43-50], we hypothesized

that neuropeptidergic pathways may isolate functionally distinct dopamine reward systems. To test this, we obtained or generated Cre-lines for these enriched neuropeptidergic genes as a method to isolate VTA subpopulations (Table 1). These distinct populations of VTA dopamine neurons provide unprecedented genetic access and a unique opportunity to manipulate discrete components of the mesolimbic dopamine system with spatial and temporal precision.

Table 1: Transgenic Cre-driver lines to isolate VTA subpopulations

Cre Driver line	Description	Status	Type	Additional Note	Reference
Slc6a3-Cre	Cre target to dopamine transporter locus	published	Knock-in Exon 1		Zhuang et al., 2005
Oprk1-Cre	Cre targeted to Kappa opioid receptor 1 locus	published	Knock-in Exon 2		Cai et al., 2016
Cck-IRES-Cre	Cre targeted to Cholecystokinin locus	published	Knock-in 3'UTR		Taniguchi et al., 2011
Tacr3-IRES-Cre	Cre targeted to tachykinin receptor 3 locus	Un-published	Knock-in 3'UTR		
Ntsr1-IRES-Cre	Cre targeted to neurotensin receptor 1 locus	Un-published	Knock-in 3'UTR	Flpable version made	
Crhr1-IRES-Cre	Cre targeted to Crhr1 receptor locus	Un-published	Knock-in 3'UTR	Flpable version made	

Results

Characterization of VTA subpopulations isolated by neuropeptidergic Cre-driver lines

To identify the neuroanatomical distribution of VTA neurons expressing each of the five neuropeptide-associated genes (*Oprk1, Ntsr1, Tacr3, Crhr1, Cck*), we injected a Cre-conditional fluorescent reporter virus (AAV1-FLEX-YFP) bilaterally into the VTA. Visual and quantitative inspection of virally-labeled cells revealed differential distribution between Cre-lines, consistent with unique subpopulations (Figure 1A-C). For *Crhr1*- and *Cck*-expressing neurons, localization was significantly biased when expression was quantified by VTA subdivision (Figure 1C). Immunohistochemical staining indicated substantial overlap between YFP and tyrosine hydroxylase (TH) for all Cre-lines, suggesting that these subpopulations are primarily dopaminergic (Figure 1D).

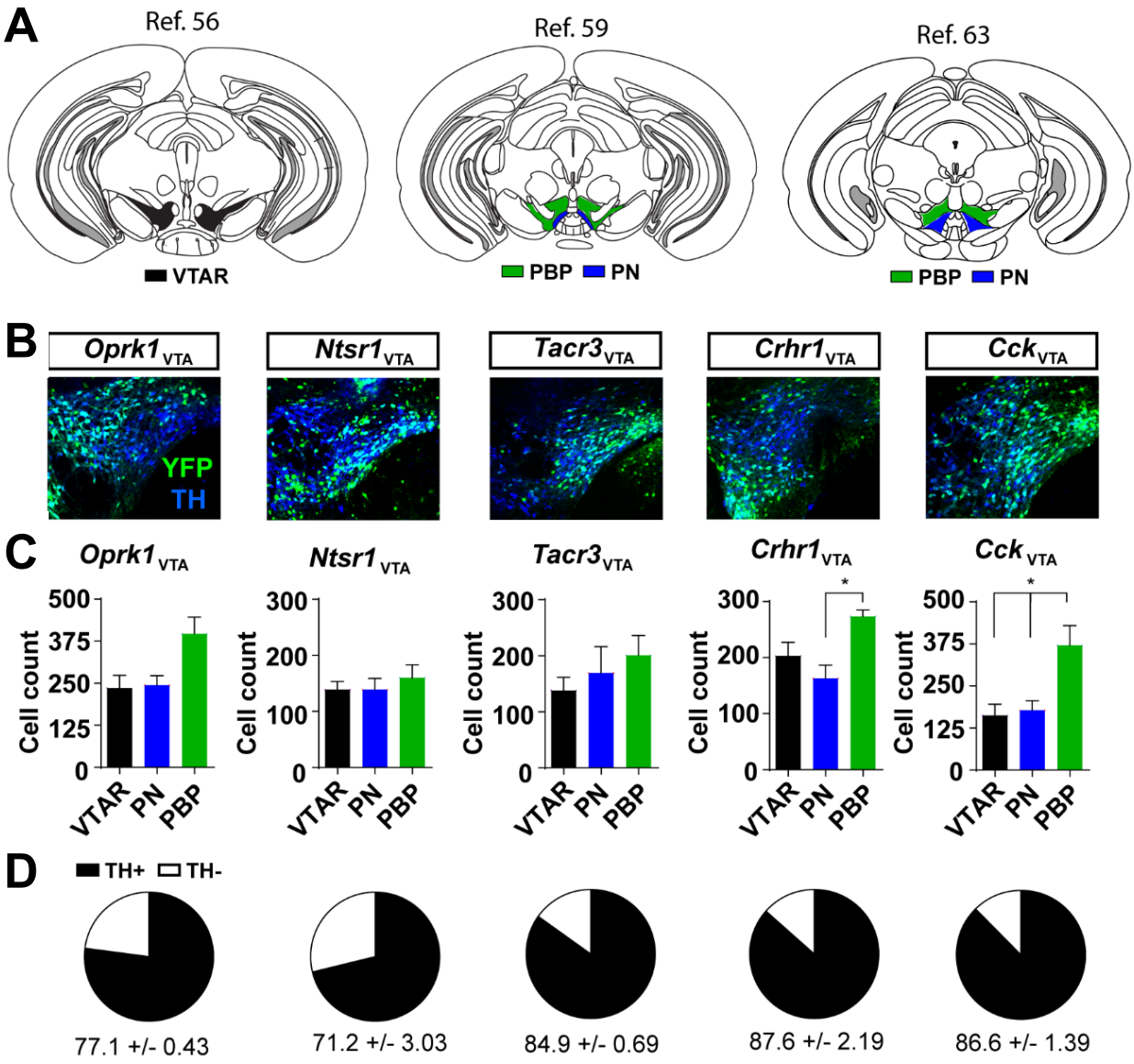

Figure 1. Anatomical characterization of VTA subpopulations. (A) Reference atlas images illustrating VTA subregions: rostral VTA (VTAR) – black; parabrachial pigmented nucleus (PBP) – green; paranigral nucleus (PN) – blue. **(B)** Example images of VTA sections co-stained for YFP (identifying VTA subpopulations after injection with AAV1-FLEX-YFP) and tyrosine hydroxylase (TH). **(C)** Cell count quantification by VTA subregion (n=3 mice, 9 sections/animal; one-way ANOVA, multiple comparisons, *P < .05). **(D)** Proportional overlap between YFP and TH.

The neuroanatomical location of dopamine neurons in the VTA is associated with projections to different output structures[38]. We next characterized the innervation profiles of these subpopulations by injection of a Cre-conditional anterograde tracer fluorescently labeled with GFP (AAV1-FLEX-Synaptophysin-GFP) into the VTA (Figure 2A-B). After allowing adequate time for axonal transport, GFP expression was assessed in the prefrontal cortex (PFC), amygdala and NAc. Only *Oprk1*$_{VTA}$ neurons had detectable projections to the PFC (Figure 3A). While all subpopulations displayed differential innervation of amygdala subregions (Figure 3B-C), the most striking distinction was in projections to NAc subregions. *Oprk1*$_{VTA}$ and *Ntsr1*$_{VTA}$ neurons broadly innervated both the core and shell. In contrast, the three remaining subpopulations displayed biased and complementary projection profiles. *Tacr3*$_{VTA}$ neurons projected to both core and shell subdivisions, but with a significant bias to the medial shell. *Crhr1*$_{VTA}$ neurons densely innervated the core with minimal innervation to shell subregions, while *Cck*$_{VTA}$ neurons displayed prominent projections to the medial shell relative to the lateral shell and core (Figure 2B-E).

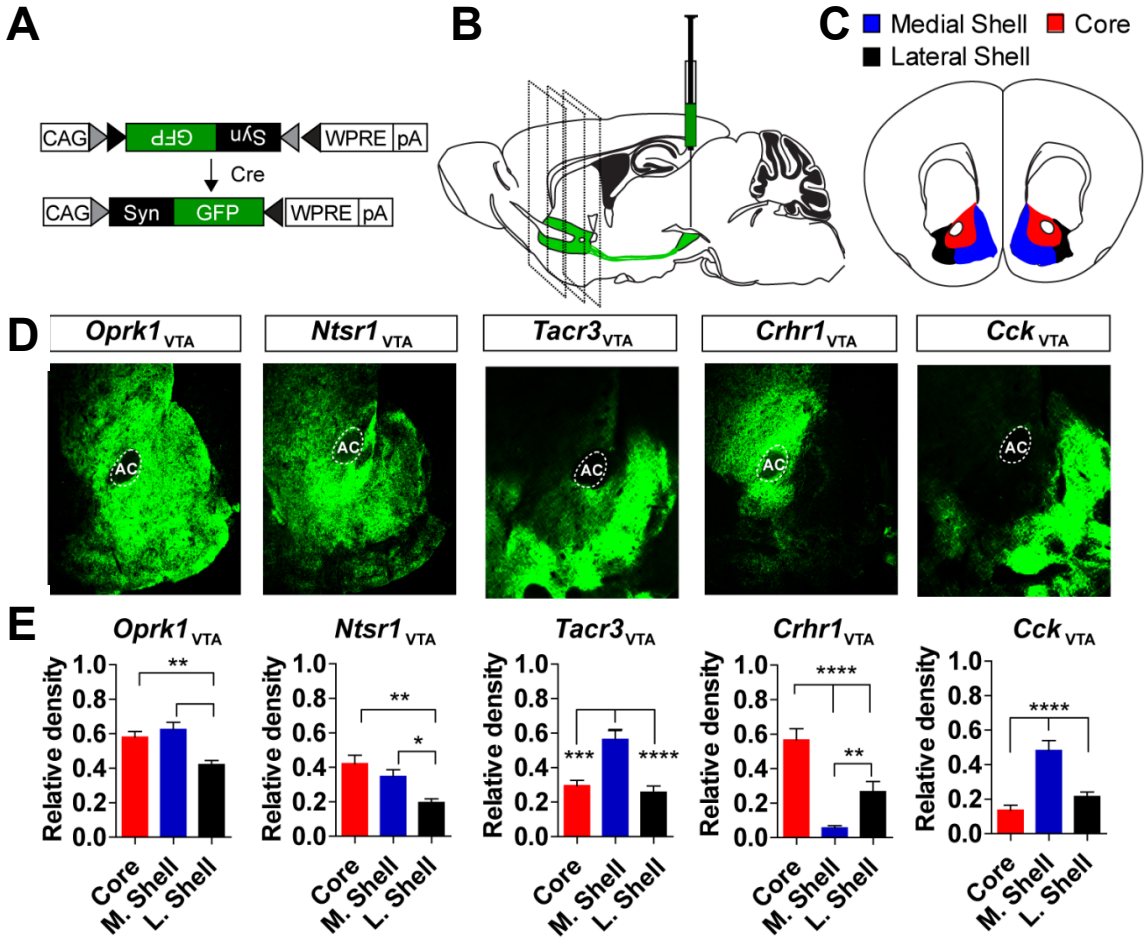

Figure 2. Isolation of divergent dopamine projection populations. (A) Schematic of AAV-FLEX-Synaptophysin-GFP. **(B)** Illustration of viral injection and sectioning of NAc. **(C)** Illustration of NAc subdivisions quantified in D and E. **(D)** Ventral striatal sections stained for synaptophysin-GFP. **(E)** Average pixel densities normalized to fluorescent intensity at the VTA injection site (*Oprk1* and *Ntsr1*: n=3 mice, 9 sections; *Tacr3*: n=4 mice, 12 sections; *Crhr1* and *Cck*: n=5 mice, 14-15 sections; *P<0.05, **P<0.01, ***P<0.001, ****P<0.0001, one-way ANOVA, Tukey's multiple comparisons). AC: Anterior commissure.

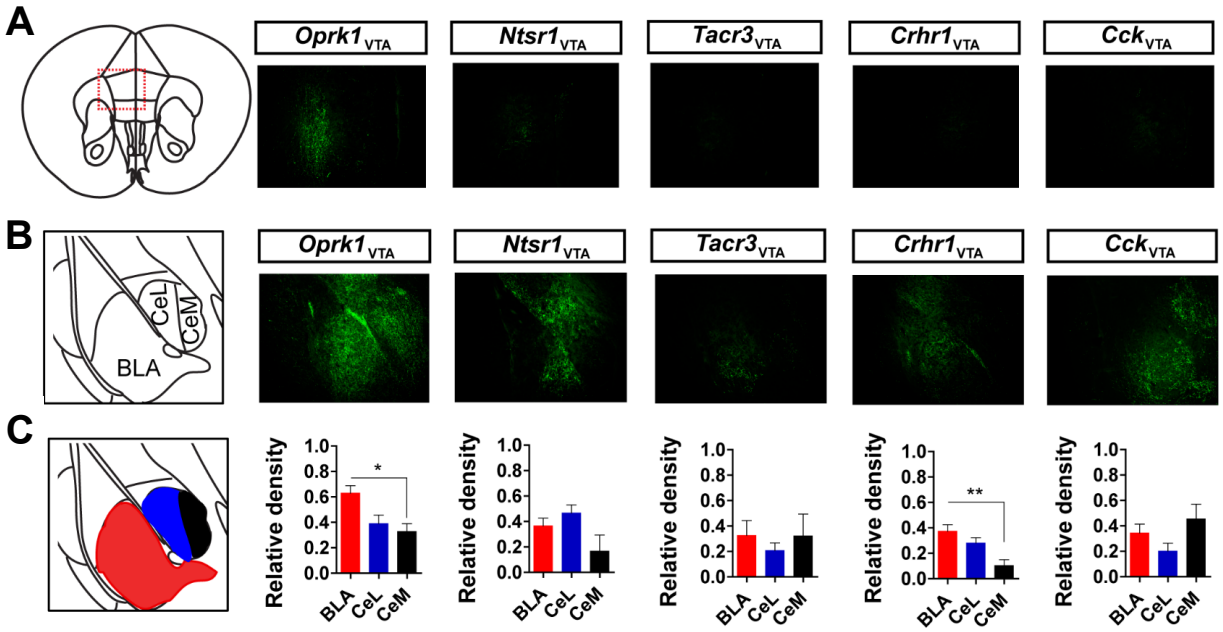

Figure 3. Subpopulation innervation of VTA-receptive brain regions. **(A)** Schematic illustrating location of dopamine input to the prefrontal cortex (left). Only $Oprk_{VTA}$ neurons showed innervation of the cortex as visualized with synaptophysin-GFP (right). **(B)** Schematic (left) illustrating location of dopamine input to the amygdala subdivisions (BLA: basolateral amygdala, CeL: central lateral nucleus, CeM: central medial nucleus). Example images (right) illustrating terminal synaptophysin-GFP expression in the amygdala. **(C)** Quantification of synaptophysin-GFP in subdivisions of the amygdala in Cre-driver lines (n=3 mice, 9 sections/animal; one-way ANOVA, multiple comparisons, *P < .05, **P < 0.01).

Synaptic connectivity profiling of VTA subpopulations

To confirm observed projection biases, we measured subpopulation- and NAc subregion-specific dopamine release using fast-scan cyclic voltammetry (FSCV) in acute striatal brain slices after injection of a Cre-conditional channel rhodopsin (ChR2) virus (AAV1-FLEX-ChR2-mCherry) into the VTA (Figure 4A). Phasic activation (3 s, 20 Hz, 5-ms pulse width) of ChR2-expressing terminals reliably evoked dopamine transients that were predominantly consistent with observed projection profiles. *Crhr1*$_{VTA}$ neurons displayed significantly biased dopamine release in the core subregion. *Cck*$_{VTA}$ terminal stimulation evoked significantly greater dopamine release in the medial shell compared to other subregions. In contrast, *Tacr3*$_{VTA}$ neurons released equivalent dopamine in the core, medial shell and lateral shell, consistent with visible projections to all three subregions, but not with a projection bias to the medial shell (Figure 4B).

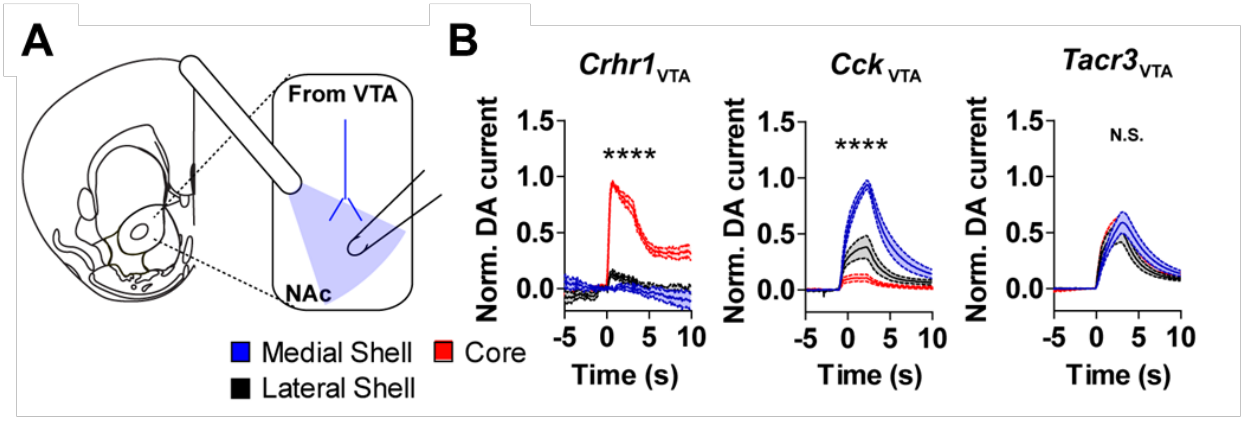

Figure 4. Biased dopamine release in NAc subregions by *Crhr1*$_{VTA}$, *Cck*$_{VTA}$ and *Tacr3*$_{VTA}$ neurons. (A) Illustration of slice voltammetry for recording optically-evoked dopamine release in NAc subregions. **(B)** Normalized dopamine current evoked by 3 seconds of 20-Hz optical stimulation of *Crhr1*$_{VTA}$, *Cck*$_{VTA}$ and *Tacr3*$_{VTA}$ ChR2-expressing terminals. Recordings from all 3 subregions were taken for each slice and normalized to the peak current amplitude per slice (*Crhr1*: n=4 mice, 9 sections; *Cck*: n=4 mice, 8 sections; *Tacr3*: n=4 mice, 15 sections, ****P<0.0001, two-way ANOVA, Bonferroni multiple comparisons).

Dopamine neurons can co-release GABA and glutamate[31,32]. To measure fast neurotransmitter release in the NAc by *Crhr1*$_{VTA}$, *Cck*$_{VTA}$ and *Tacr3*$_{VTA}$ neurons, we recorded post-synaptic responses in all three subregions following optical stimulation of ChR2-expressing terminals (Figure 5A). We observed a heterogeneous array of responses that were primarily consistent with mapped projection biases. *Cck*$_{VTA}$ neuron stimulation resulted in glutamate-driven responses (optically-evoked excitatory post-synaptic currents (oEPSCs) and feed-forward inhibition) in the medial shell, but also optically-evoked inhibitory post-synaptic currents (oIPSCs) in the lateral shell. No connectivity was observed in the core. *Crhr1*$_{VTA}$ terminal stimulation produced oIPSCs in the core with no effect in shell subregions. *Tacr3*$_{VTA}$ neurons displayed excitatory connectivity in the medial shell with few responses seen in the core and lateral shell subregions (Figure 5B-C). Collectively, these subpopulations display biased connectivity primarily in accordance with descriptive mapping results, and demonstrate that several neurotransmitter systems are operating within VTA to NAc circuit pathways.

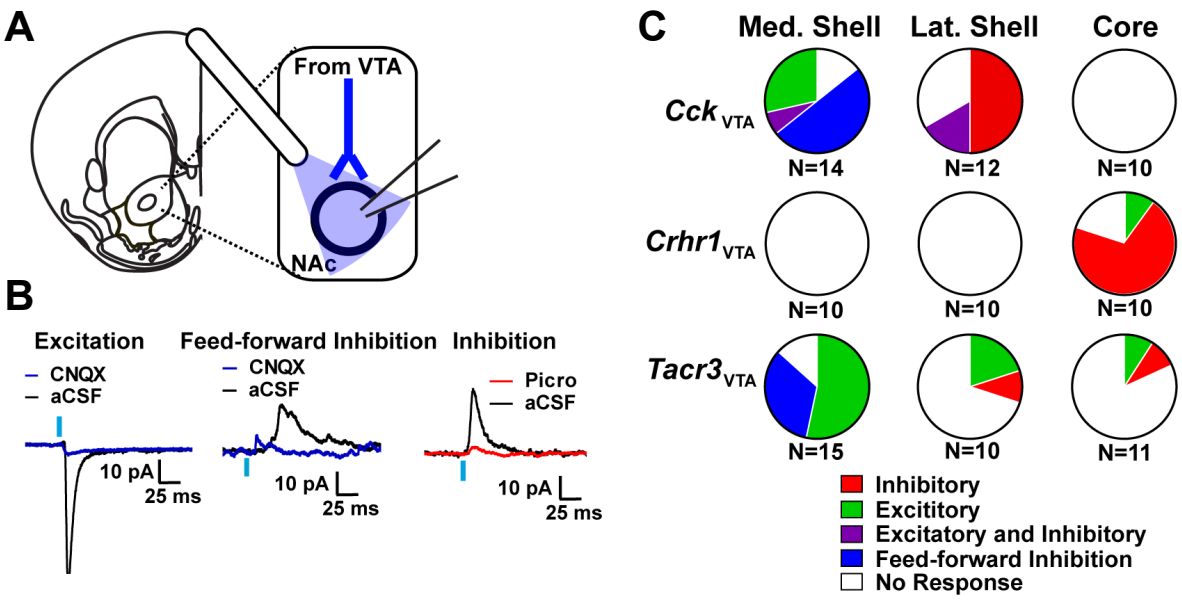

Figure 5. GABA and glutamate connectivity of distinct dopamine populations. (A) Schematic for recording optically evoked post-synaptic responses in NAc subregions. **(B)** Example traces for *Tacr3* oEPSC (left), *Cck* feed-forward inhibition (middle), and *Crhr1* oIPSC (right). **(C)** Postsynaptic response proportions following stimulation of Cck_{VTA}, $Crhr1_{VTA}$ and $Tacr3_{VTA}$ terminals.

Characterization of VTA subpopulation intrinsic physiology

The intrinsic electrophysiological properties of VTA dopamine neurons have been shown to cluster into two distinct groups based on projection target[38]. To assess a subset of these properties in *Crhr1*$_{VTA}$, *Cck*$_{VTA}$ and *Tacr3*$_{VTA}$ neurons, we injected a Cre-conditional fluorescent reporter virus into the VTA to identify neurons for subsequent analysis through *ex vivo* patch-clamp electrophysiology. We measured baseline firing rate (Figure 6A-C, M), hyperpolarization-activated cation current (I_h) (Figure 6D-F, K), repolarization-induced tail current (Figure 6G-I, L) and resting membrane potential (Figure 6J). Consistent with each subpopulation demonstrating multiple projection targets that fall into both physiological clusters, we observed a broad distribution for each measure. No significant differences were identified between subpopulations. Almost all neurons tested were sensitive to D2-receptor mediated inhibition (Figure 6A-C), consistent with TH immunoreactivity analysis that these subpopulations are predominantly dopaminergic (Figure 2D).

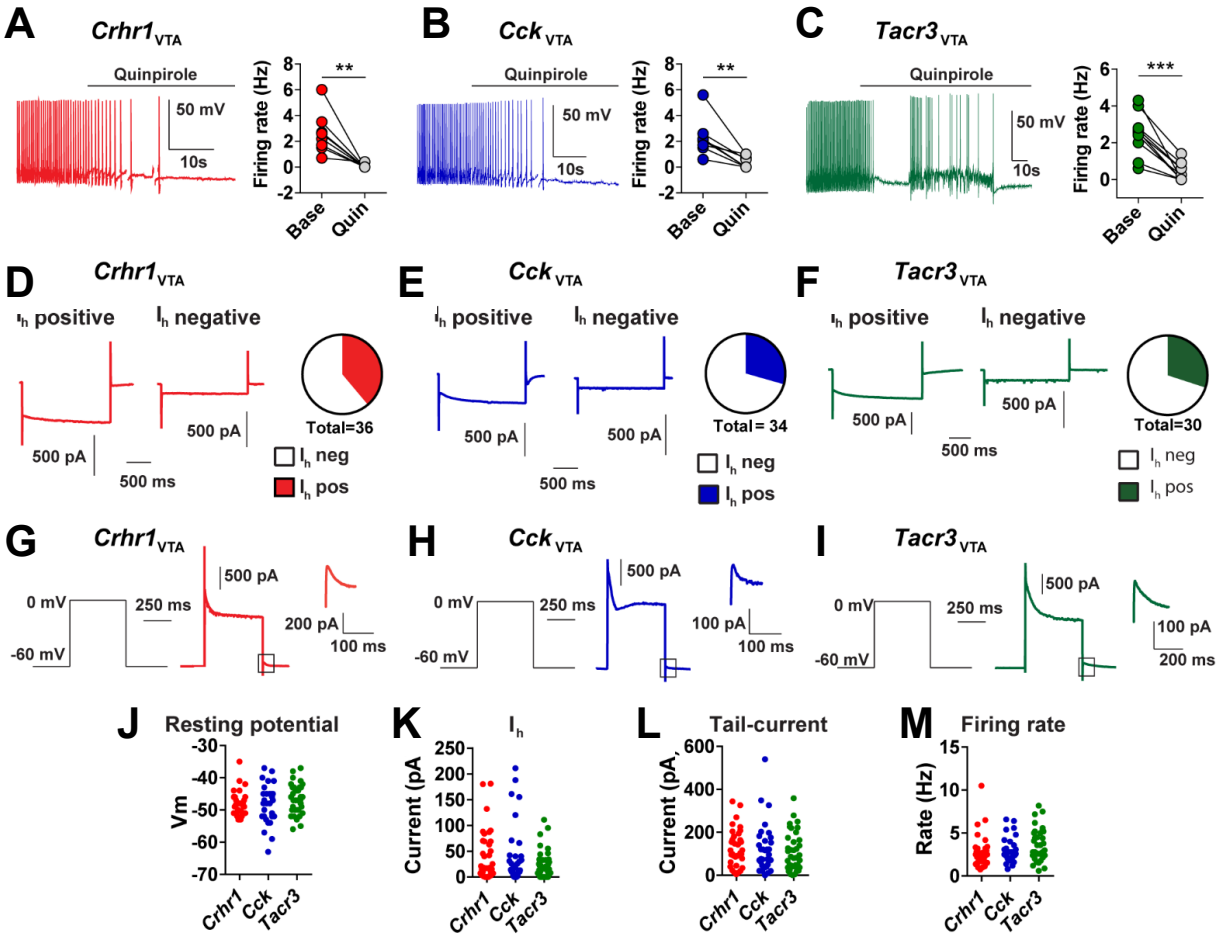

Figure 6. Characterization of *Crhr1*$_{VTA}$, *Cck*$_{VTA}$, and *Tacr3*$_{VTA}$ intrinsic physiological properties. (A-C) Left: Example traces illustrating sensitivity to the D2 agonist Quinpirole (1 mM). Right: Firing rate before and after Quinpirole application. (*Crhr1* (k): n=3 mice, 8 cells; *Cck* (l): n=3 mice, 8 cells; *Tacr3* (m): n=2 mice, 10 cells; student's paired t-test, two-tailed, **P < 0.01, ***P < .001). **(D-F)** Example traces for hyperpolarization-activated (I_h) current positive (left trace) and negative (right trace) for *Crhr1*$_{VTA}$ (D), *Cck*$_{VTA}$ (E), or *Tacr3*$_{VTA}$ (F) neurons. Pie chart (right) quantifies proportion of I_h positive or negative neurons (*Crhr1*: n=6 mice, 36 cells; *Cck*: n=6 mice, 34 cells, *Tacr3*: n=5 mice, 30 cells). **(G-I)** Tail current voltage-step protocol and example current trace for *Crhr1*$_{VTA}$ (G), *Cck*$_{VTA}$ (H), or *Tacr3*$_{VTA}$ (I) neurons. Inset: magnified current trace highlighted by black box. (**J)** Resting membrane potential (*Crhr1*: n=6 mice, 32 cells; C*ck*: n=6 mice, 30 cells; *Tacr3*: n=5 mice, 37 cells). **(K)** I_h current quantified from D-F. **(L)** Tail current quantified from G-I (*Crhr1*: n=6 mice, 35 cells; *Cck*: n=6 mice, 34 cells; *Tacr3*: n=5 mice, 38 cells). **(M)** Firing rate of neurons recorded in D-F.

Genetic isolation of distinct VTA populations for functional interrogation

This characterization indicates that neuropeptide-associated gene expression can isolate unique subpopulations of VTA dopamine populations. Projection and connectivity analysis reveals subpopulation-specific innervation of discrete output targets and a strategy for interrogation of dopamine sub-system function. *Crhr1*$_{VTA}$ and *Cck*$_{VTA}$ neurons, based on differential innervation of NAc and amygdala subregions (Figure 2-5), likely represent the most distinct subpopulations. To directly assess the overlap between these two populations, we preformed RNAscope *in situ* hybridization probing for *Crhr1* and *Cck* mRNA transcripts in VTA brain slices. These two VTA populations were 75% non-overlapping and were differentially located within VTA subregions (Figure 7A-D). Genetic isolation of these populations with segregated projections provides direct access to probe how these neurons encode reward-related information and their roles in orchestrating specific reward processes.

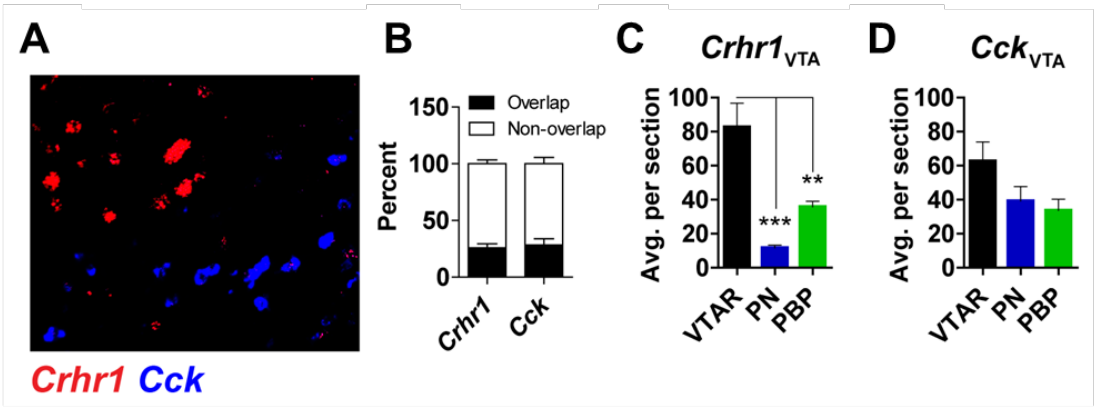

Figure 7. Crhr1 and Cck represent primarily distinct VTA populations. (A-B) Quantification of overlap between *Crhr1*$_{VTA}$ and *Cck*$_{VTA}$ neurons (n=5 mice, 13 sections). **(C-D)** Cell count by VTA subregion (n=5 mice, 13 sections (10-µm); one-way ANOVA, multiple comparisons, **P < .01, ***P < .001).

Reward encoding by Crhr1$_{VTA}$ and Cck$_{VTA}$ neurons in vivo

Dopamine neurons encode reward-related information through dynamic changes in activity[2]. To measure if and how *Crhr1*$_{VTA}$ and *Cck*$_{VTA}$ populations respond to reward-predictive cues, actions and receipt, we performed *in vivo* tetrode recordings using the optical-tagging strategy[51]. *Crhr1*-Cre and *Cck*-Cre mice were injected with AAV1-FLEX-ChR2-mCherry unilaterally into the VTA and implanted with drivable optrodes (Figure 8A). Cells were identified as either *Crhr1* or *Cck* for recording based on short-latency and high-fidelity spiking following optical stimulation (Figure 8B-C). Mice were trained on a simple instrumental conditioning paradigm (fixed ratio, FR1) consisting of three events: lever extension (cue presentation indicating active trial), action (lever press) and reward receipt (head entry into the food hopper to retrieve food pellet) (Figure 8D).

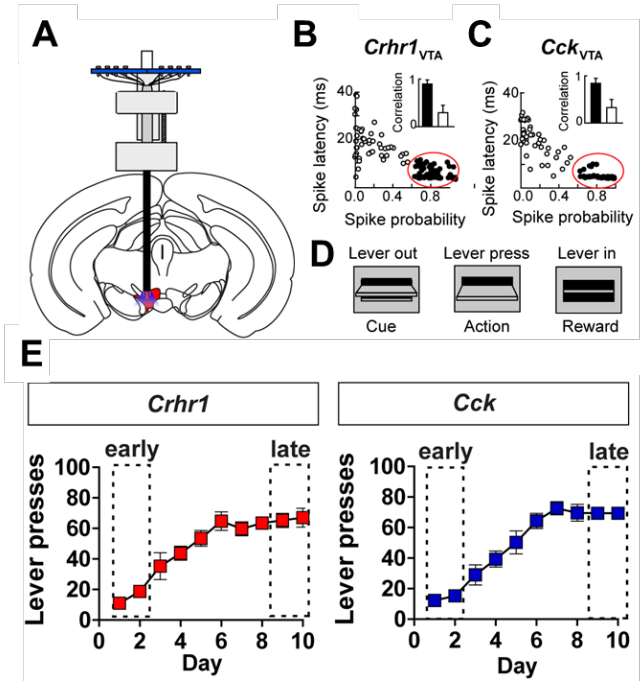

Figure 8. *In vivo* recording and conditioning paradigm. (A-C) Optical identification of neurons during *in vivo* tetrode recording. Neurons with short-latency, high-fidelity responses to light (filled circles) were characterized as either *Crhr1*$_{VTA}$ (B) or *Cck*$_{VTA}$ (C) neurons. Inset: action potential waveform correlation between light-evoked and spontaneous action potentials. **(D)** Schematic of the 3 events comprising the instrumental conditioning paradigm. **(E)** Lever presses/day by *Crhr1* and *Cck* groups over 10 days of recording during FR1 instrumental conditioning (*Crhr1*: n=4 mice; *Cck*: n=3 mice).

After two days of conditioning to establish a minimal level of responding, neurons were recorded over the 10 subsequent training days. We observed subtle changes in responses over the course of conditioning. To further resolve these adaptations, we analyzed responses during early conditioning (low lever pressing: days one and two of recording) and late conditioning (high lever pressing: days nine and 10 of recording) (Figure 8E). During early conditioning, both populations exhibited phasic activation to all three events with no differences in the amplitude of these dynamics or proportion of responsive cells (Figure 9A-C). We also observed an elevation in baseline firing rate beginning prior to lever press and persisting until reward receipt for both *Crhr1*$_{VTA}$ and *Cck*$_{VTA}$ neurons (Figure 9D). In contrast to the response similarity observed during early conditioning, significant differences in these populations emerged during late conditioning. Action- and reward-responsive neurons represented a significantly larger proportion of the population of *Crhr1*$_{VTA}$ compared to *Cck*$_{VTA}$ neurons (Figure 9E-F). The proportion of cue-responsive neurons did not differ, and no significant differences in the phasic activation of responsive neurons were observed (Figure 9F-G). Only *Cck*$_{VTA}$ neurons exhibited the tonic rise in baseline activity in pursuit of reward, unlike during early conditioning when this response feature was observed in both populations (Figure 9H). No differences in baseline *in vivo* electrophysiological properties including firing rate, burst rate and spikes per burst were observed (Figure 10A-C).

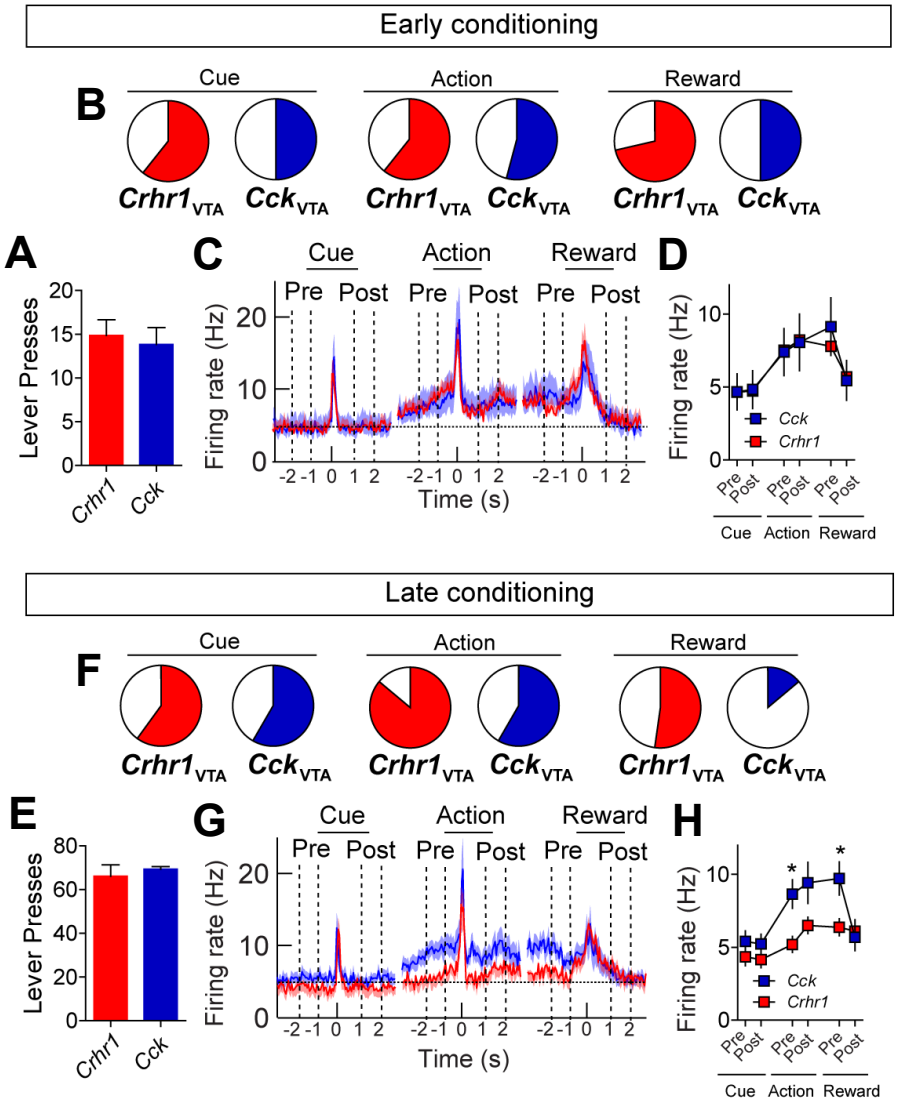

Figure 9. Reward encoding by *Crhr1*$_{VTA}$ and *Cck*$_{VTA}$ populations. (A and E) Lever presses over the one-hour conditioning sessions during recording days one and two (early conditioning) or days nine and ten (late conditioning). **(B and F)** Proportion of responsive cells to each of the three events (*Crhr1*-Cre: n=4 mice, 28 cells early conditioning and 13 cells late conditioning; *Cck*-Cre: n=3 mice, 24 cells early conditioning and 24 cells late conditioning) was significantly different during late conditioning (F, *P<0.01, *Chi*-square). **(C and G)** Average firing rate across reward trials. Time zero signifies event onset. **(D and H)** Firing rate during different trial stages demonstrates a tonic rise in neural activity; 1-s peri-event bins indicated by 'Pre' and 'Post' stimulus in (C and G) were used to calculate average firing rate immediately preceding or following cue, action or reward events (*P<0.05, two-way ANOVA, Bonferroni multiple comparisons).

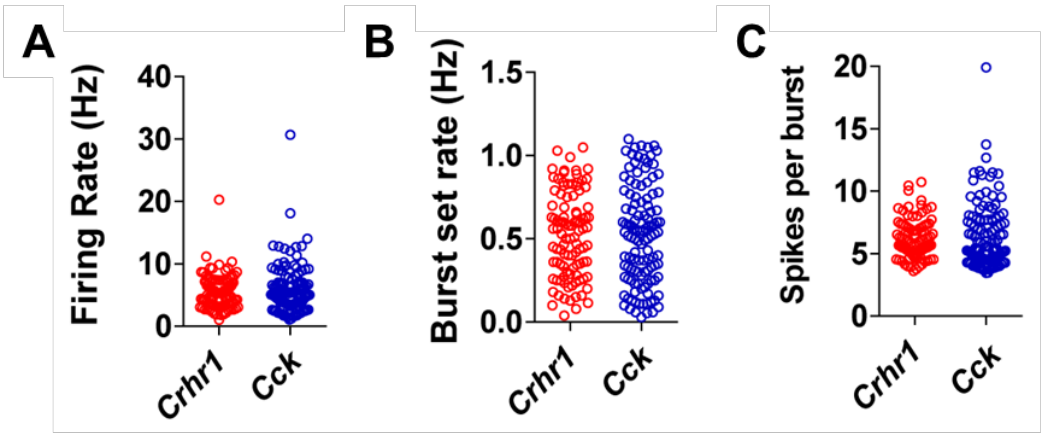

Figure 10. Baseline in vivo firing properties of *Crhr1*$_{VTA}$ and *Cck*$_{VTA}$ neurons. (A-C) Basal *in vivo* firing properties including baseline firing rate (A), burst set rate (B) and spikes per burst (C) (*Crhr1*: n=4 mice, 100 cells; *Cck*: n=3 mice, 117 cells).

Differential regulation of reward processes by Crhr1$_{VTA}$ and Cck$_{VTA}$ neurons

Based on differences in NAc innervation and electrophysiological response adaptations during instrumental conditioning, we next asked whether *Crhr1*$_{VTA}$ and *Cck*$_{VTA}$ neurons coordinate distinct reward processes. We first tested the sufficiency of these two populations to promote response-outcome contingencies by time-locking optogenetic phasic stimulation (3 s, 20 Hz, 5-ms pulse width) with lever press in lieu of food reward in the same instrumental paradigm as above. Mice were injected with AAV1-FLEX-ChR2-mCherry and implanted with an optic fiber unilaterally in the VTA prior to five days of training (Figure 11). Interestingly, only *Crhr1*$_{VTA}$ activation facilitated the acquisition of instrumental responding, as *Cck*-Cre animals were not different than controls (Figure 12A). Given the modest level of responding by *Crhr1*-Cre mice, we next investigated how this compared to stimulation of most VTA dopamine neurons using the DAT (*Slc6a3*)-Cre line. Consistent with previous studies[52,53], optogenetic stimulation of DAT$_{VTA}$ neurons resulted in rapid acquisition and high levels of operant responding (Figure 12A).

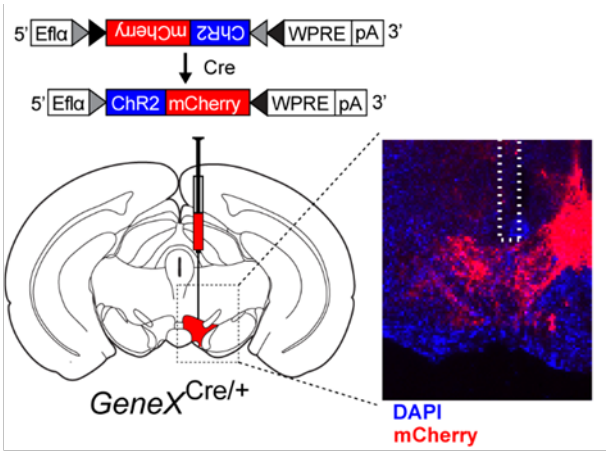

Figure 11. Optogenetic stimulation approach. Left: schematic of AAV1-FLEX-ChR2-mCherry injected into the VTA of Cre-driver lines. Right: Immunohistochemical staining for mCherry demonstrating expression in the VTA and optic fiber placement (white dashed lines).

We next asked whether the response profiles observed would change if the mice had already established a reward contingency (Figure 12B). Mice were trained to lever press for food reward for 5 days before transitioning to 5 days of optogenetic stimulation. *Crhr1*-Cre, *Cck*-Cre and control groups all learned to lever press for food reward over the first 5 days of training and exhibited an extinction-like burst in responding on the first day after switching to optical stimulation. However, this increase in lever pressing was significantly greater for *Cck*-Cre mice and remained elevated over the four subsequent optical-stimulation days. In contrast, *Crhr1*-Cre and control groups both exhibited a gradual extinction of responding, returning close to food reward levels by the last day of training (Figure 12B).

One interpretation of these data is that *Cck*$_{VTA}$ neurons cannot promote the formation of action-outcome associations, but are highly motivating once an association has been learned. To further probe the function of *Cck*$_{VTA}$ or *Crhr1*$_{VTA}$ activation, we asked how optical stimulation of these subpopulations compared to natural food reward. Food-restricted mice were first trained to press either of two levers for a food reward. After three days, one lever remained paired with food while the other was switched to provide optical stimulation when pressed for three subsequent days. We again observed divergent behaviors between the two groups. *Crhr1*-Cre mice significantly preferred the food-paired lever, while *Cck*-Cre mice significantly preferred the optical stimulation-paired lever (Figure 12C). To more directly test motivation, we performed a progressive ratio assay[54] in which the number of responses required to receive optical stimulation increases non-arithmetically over the course of the session. *Cck*-Cre and DAT-Cre mice had significantly higher break points (number of presses in the last successfully completed ratio) than the mCherry control group, consistent with a motivational component of activation. *Crhr1*-Cre and control groups were not different (Figure 12D).

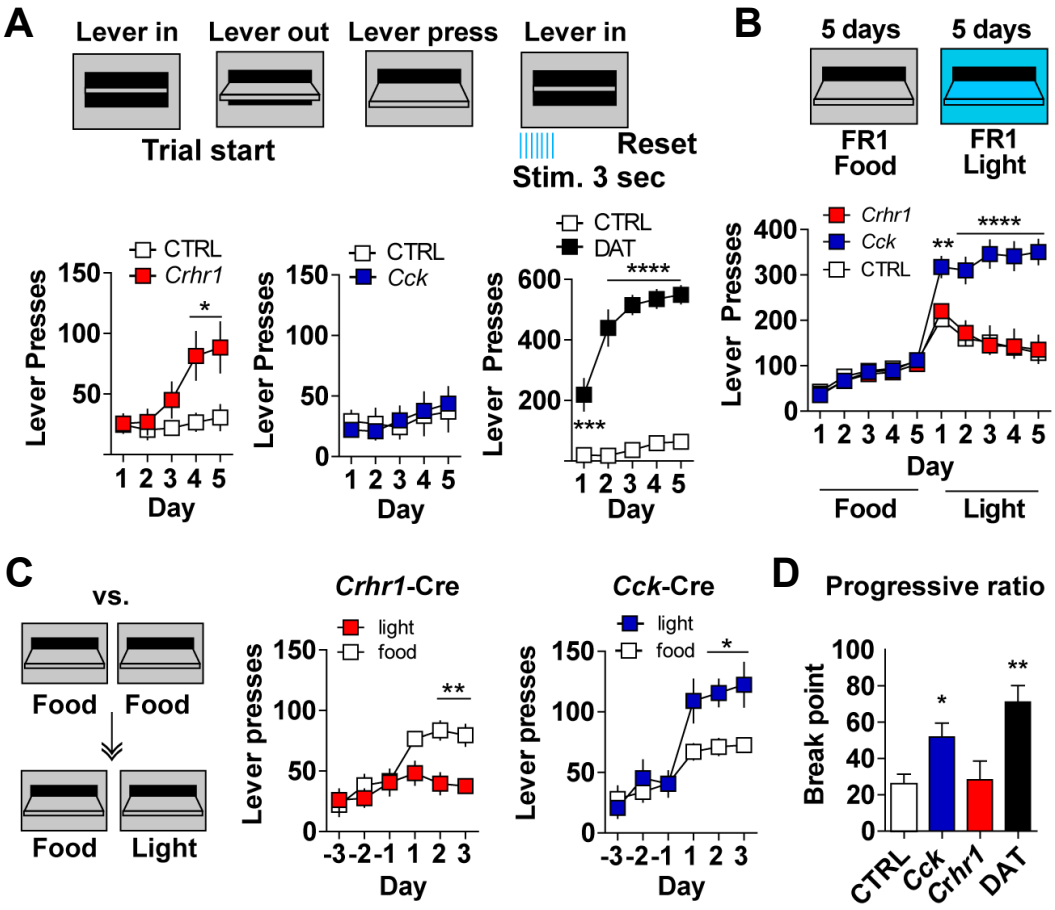

Figure 12. *Crhr1*$_{VTA}$ and *Cck*$_{VTA}$ neurons are operationally distinct. (A) Top: schematic of instrumental conditioning paradigm for optical stimulation. Each lever press resulted in immediate stimulation (3 s, 20 Hz, 5-ms pulse width) and a 5-s timeout before lever re-extension. Bottom: lever presses/day for *Crhr1*-Cre (left, n=9), *Cck*-Cre (middle, n=16) and DAT-Cre (right, n=6) over 5 days of training. Control AAV1-FLEX-mCherry groups for each line are shown in white (n=6 for DAT-Cre and *Crhr1*-Cre, n=8 for *Cck*-Cre) (*P<0.05, ***P<0.001, ****P<0.0001, Two-way ANOVA, Bonferroni multiple comparisons). **(B)** Top: schematic illustrating 5 days of instrumental conditioning for food reward followed by 5 days for optical stimulation paradigm. Bottom: Lever presses/day for *Crhr1*-Cre, *Cck*-Cre and control groups (*Crhr1* and control: n=8 mice, *Cck*: n=7 mice) (**P< 0.01, ****P<0.0001, two-way ANOVA, Bonferroni multiple comparisons). **(C)** Schematic of food reward vs. optogenetic stimulation paradigm (left). Mice underwent 3 days (days -3 through -1) of FR1 instrumental conditioning for food reward. On days 1 through 3, one lever was switched to give stimulation (3 s, 20 Hz, 5-ms pulse width). *Crhr1* (middle) and *Cck* (right) lever presses/day on food- and light-paired levers (*Crhr1*: n=6 mice; *Cck*: n=8 mice) (*P< 0.05, **P<0.001, two-way ANOVA, Bonferroni multiple comparisons). **(D)** Average break points on progressive ratio task (control: n=18 mice; *Cck*: n=16 mice; *Crhr1*: n=17 mice; DAT: n=8 mice) (*P<0.05, **P<0.001, one-way ANOVA, Bonferroni selected comparisons to controls).

Determining the dopamine dependence of Cck_{VTA} and $Crhr1_{VTA}$ mediated reward behaviors

The wealth of evidence linking dopamine and reward behavior strongly suggests that the acquisition and maintenance of instrumental responding mediated by $Crhr1_{VTA}$ and Cck_{VTA} neuron activation, respectively, is dependent on target-specific dopamine release. However, we demonstrated that $Crhr1_{VTA}$ and Cck_{VTA} neurons can co-release GABA and glutamate. To determine if the observed behaviors for each population are dependent on dopamine and not another neurotransmitter system, we applied intersectional genetic strategies to selectively inactivate *Th*, the enzyme in the rate-limiting step in dopamine synthesis in either Cck_{VTA} or $Crhr1_{VTA}$ neurons. To accomplish this, *Cck*-Cre mice were crossed with Th^{lox} mice[55] to generate *Cck*-Cre::$Th^{lox/lox}$ and *Cck*-Cre::$Th^{lox+/}$ mice. *Cck* expression does not overlap with *Th* expression in other neuronal populations[56,57] Consistent with this, TH immunoreactivity was reduced in the VTA but did not alter expression in the locus coeruleus in *Cck*-Cre::$Th^{lox/lox}$ mice (Figure 13A). We further validated this approach by quantifying overlap between TH and Cre-conditional mCherry (AAV1-FLEX-ChR2-mCherry) expression. Consistent with selective *Th* inactivation and ChR2 expression, there was significantly less overlap in *Cck*-Cre::$Th^{lox/lox}$ than *Cck*-Cre::$Th^{lox/+}$ mice (Figure 13B). Behavioral testing in these mice demonstrated that dopaminergic transmission is necessary to drive the elevation and sustained increase in responding following the switch from food reward to optical stimulation (Figure 13C).

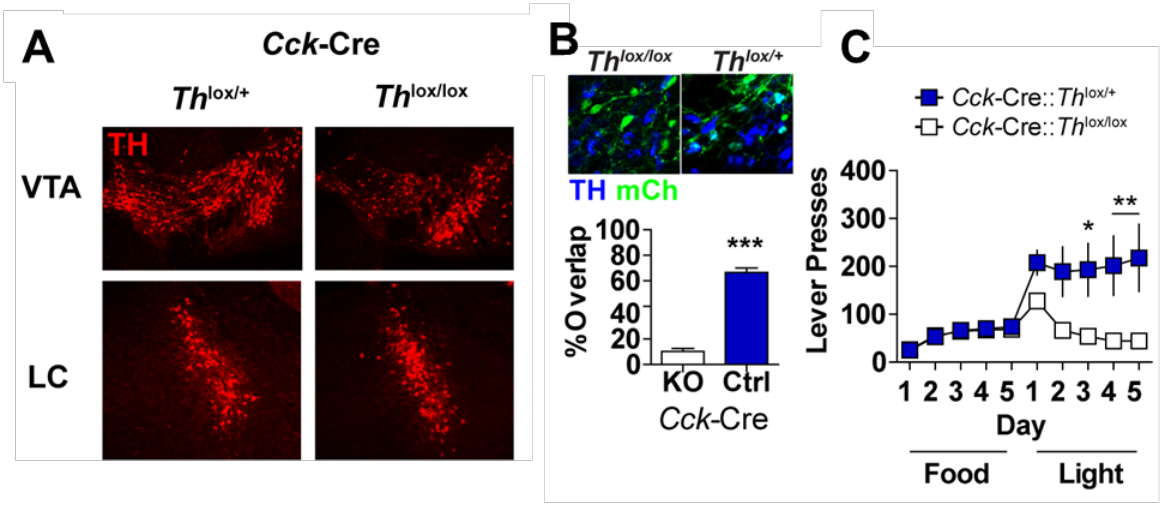

Figure 13. *Th* inactivation in *Cck*-Cre mice. (A) Biallelic *Th* excision in *Cck*-Cre mice results in reduced TH expression in the VTA (top), but no loss in the locus coeruleus (LC: bottom). **(B)** Co-staining for TH (blue) and mCherry (green) in *Cck*-Cre::$Th^{lox/lox}$ or *Cck*-Cre::$Th^{lox/+}$ mice injected with AAV1-FLEX-ChR2-mCherry (n=3 mice, 2-4 sections/animal, ***P<0.001, student's t-test unpaired). **(C)** Lever presses/day during FR1 for food reward followed by FR1 for optogenetic stimulation conditioning paradigm (lox/+: n=7 mice; lox/lox: n=6 mice, *P<0.05, **P<0.01, two-way ANOVA, Bonferroni multiple comparisons).

In contrast to *Cck*, *Crhr1* is expressed in TH neurons of the LC[58]. To prevent the inactivation of *Th* in this population, we generated a Flp recombinase-dependent Cre *Crhr1* line (*Crhr1*-frtFLEX-Cre). Injection of AAV1-Flp-dsRed into the VTA results in activation of Cre recombinase (Figure 14A) and conditional inactivation of *Th* in $Crhr1_{VTA}$ neurons. We again observed a significant reduction in overlap between TH and mCherry in *Crhr1*-frtFLEX-Cre::$Th^{lox/lox}$ compared to *Crhr1*-frtFLEX-Cre::$Th^{lox/+}$ mice after co-injection of AAV1-Flp-dsRed and AAV1-FLEX-ChR2-mCherry into the VTA (Figure 14B). Selective elimination of dopamine synthesis in $Crhr1_{VTA}$ neurons abolished the acquisition of instrumental responding for light stimulation (Figure 14C).

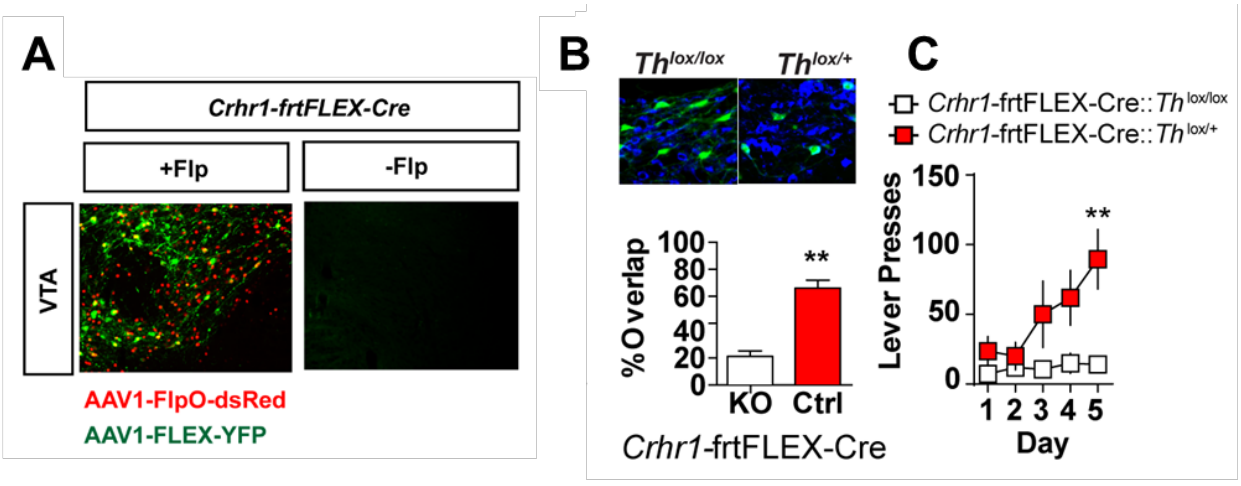

Figure 14. *Th* inactivation in *Crhr1*-frtFLEX-Cre mice. (A) Injection of AAV1-FlpO-dsRed turns on Cre-recombinase allowing for conditional gene inactivation and expression. **(B)** Co-staining for TH and ChR2-mCherry in *Crhr1*-frtFLEX-Cre::$Th^{lox/lox}$ or *Crhr1*-frtFLEX-Cre::$Th^{lox/+}$ mice (n=3 mice, 2-4 sections/animal, **P<0.01, student's t-test unpaired). **(C)** Lever presses/day during FR1 for optogenetic stimulation conditioning paradigm (n=7 mice/group, ***P<0.001, two-way ANOVA, Bonferroni multiple comparisons).

Probing the necessity of Crhr1$_{VTA}$ and Cck$_{VTA}$ in reward association

Results thus far with ChR2-mediated activation suggest that *Crhr1*$_{VTA}$ neurons provide a learning signal that helps form action-outcome associations, but are not highly motivating. In opposition to this, *Cck*$_{VTA}$ neurons cannot facilitate the formation of an action-outcome contingency but provide a robust motivational signal once an association is established. To further probe how these populations contribute to reward association, we performed temporally precise, bilateral optogenetic inhibition with the red-shifted inhibitory opsin Jaws (AAV1-FLEX-Jaws-GFP) during a non-contingent Pavlovian conditioning paradigm (Figure 15A-B). Three seconds of inhibition (2-s pulse, 1-s ramp down) were paired with lever extension/retraction (CS) that co-terminated with food pellet reward delivery (US) (Figure 15B). Conditioned-approach behavior was measured by head-entry rate into the site of reward delivery during both the CS presentation and the inter-trial interval (ITI). Inhibition time-locked to CS presentation significantly attenuated the CS-evoked head entry rate of *Crhr1*-Cre and DAT-Cre groups compared to the mCherry control group (Figure 15C). We also observed a small, but significant reduction in ITI head entry rate in the DAT-Cre group only (Figure 15D). There were no differences between *Cck*-Cre and control groups. We next assayed the ability of Pavlovian conditioning to promote sign-tracking behavior by making food pellet reward contingent on lever press without any optogenetic manipulation (Figure 15E). On the first day of the instrumental-response phase, *Crhr1*-Cre and DAT-Cre mice performed significantly fewer lever presses than controls. However, these groups were able

to learn the contingency and reached control levels of responding by day three. Again, no differences were observed between *Cck*-Cre and control mice (Figure 15G).

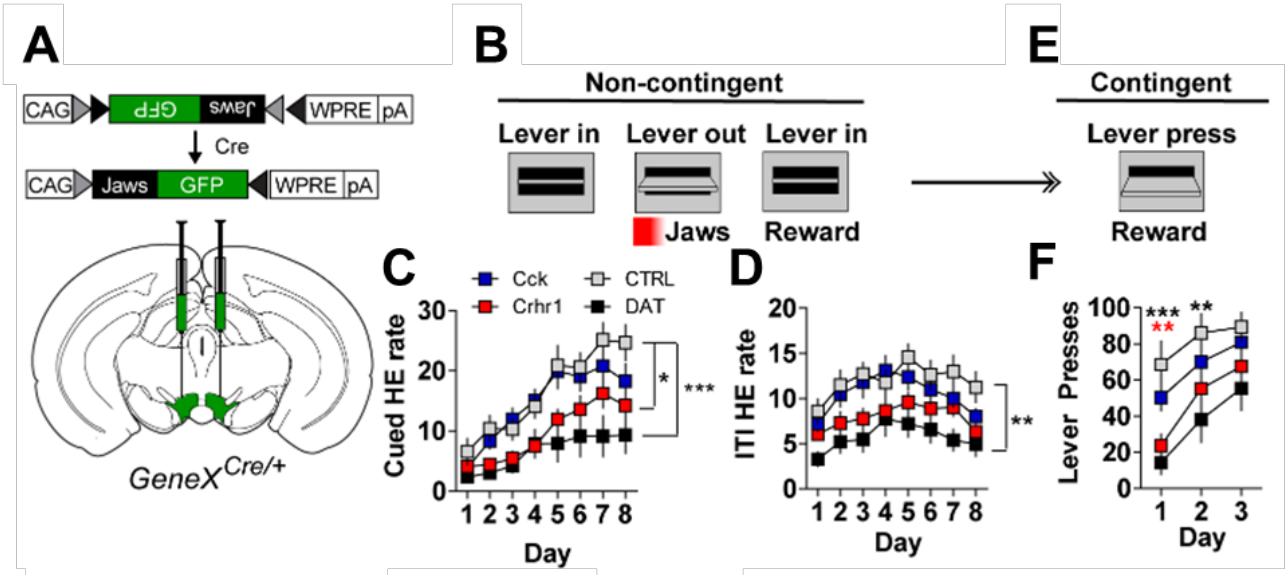

Figure 15. Jaws-mediated inhibition of Crhr1VTA and DAT-CreVTA neurons reduces conditioned approach and sign-tracking behavior. (A) Schematic of AAV1-FLEX-Jaws-GFP injected bilaterally into the VTA to inhibit $Crhr1_{VTA}$, Cck_{VTA}, or DAT_{VTA} neurons. **(B)** During Pavlovian conditioning optogenetic inhibition was paired with CS onset. Each 10-s CS presentation was immediately followed by food pellet delivery. **(C)** Head entry rate (per min) into the food hopper during 10-s CS presentation over 8 days of conditioning ($Crhr1_{VTA}$ and Cck_{VTA}: n=12 mice/group; DAT_{VTA}: n=9, *P<0.05, **P<0.01, Two-way ANOVA, Bonferroni selected comparison to controls). **(D)** Head entry rate (per min) into the food hopper during the inter-trial interval over 8 days of conditioning in the same mice (*P<.05, Two-way ANOVA, Bonferroni selected comparisons to controls). **(E)** Schematic for FR1 instrumental conditioning following 8 days of Pavlovian conditioning. **(F)** Lever presses/day over 3 days of instrumental conditioning (*P<0.05, ***P<0.001, Two-way ANOVA, Bonferroni selected comparisons to controls).

To assess whether an intrinsic aversion from optical inhibition was responsible, in part, for the diminished approach and sign-tracking behavior of *Crhr1*-Cre and DAT-Cre mice, we performed a real-time place preference assay, pairing one side of a two-chamber apparatus with continual inhibition. Only DAT-Cre mice developed an aversion for the light-paired side, an effect not observed in control, *Cck*-Cre or *Crhr1*-Cre cohorts (Figure 16).

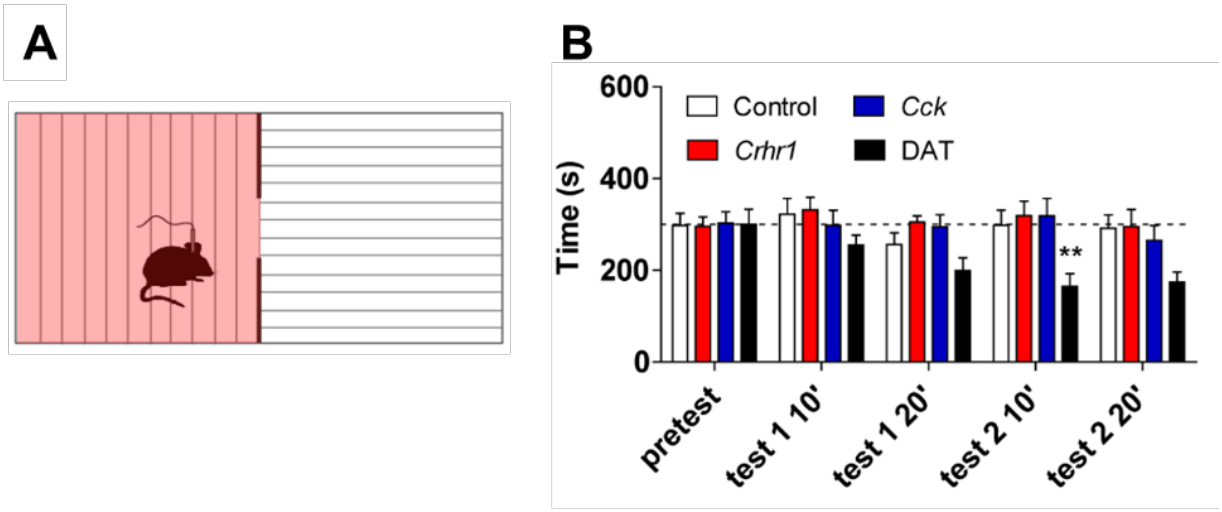

Figure 16. Real-time place aversion assay with Jaws-mediated inhibition. (A) Schematic of behavioral apparatus. One side of the two-chamber box was paired with continuous optical inhibition (2-s pulse, 1-s ramp down, 1 s off). **(B)** Real-time place preference assay with optical inhibition (*Crhr1*, *Cck* and control: n=12 mice/group; DAT: n=9, **P<.01, Two-way ANOVA, Bonferroni selected comparisons to control).

Convergent function of associative and motivational dopamine sub-systems

Our data suggest dopamine populations with distinct mesolimbic connectivity orchestrate discrete associative and motivational reward processes (Figure 17A). We hypothesized that the coordinated activation of these systems is sufficient to maximize reward reinforcement. To test this, we generated double transgenic *Crhr1*-Cre::*Cck*-Cre mice and tested their behavior in an FR1 schedule of reinforcement for optical activation of both populations. These mice exhibited rapid acquisition and high levels of responding over five training days (Figure 17B). *Tacr3*-Cre mice demonstrated similarly high reinforcement behavior (Figure 17B). *Tacr3*-expressing neurons represent a significantly smaller number of VTA neurons than either *Crhr1* or *Cck* (Figure 17C), suggesting that maximal reinforcement behavior is not due to an increase in the number of stimulated cells, but likely due to co-activation of core- and shell-projecting dopamine pathways. Similarly, *Tacr3*-Cre, *Crhr1*-Cre::*Cck*-Cre and DAT-Cre mice all demonstrated a significant place preference for an optical-activation paired chamber in the real-time place preference assay, an effect not observed in *Crhr1*-Cre or *Cck*-Cre groups (Figure 17D-E).

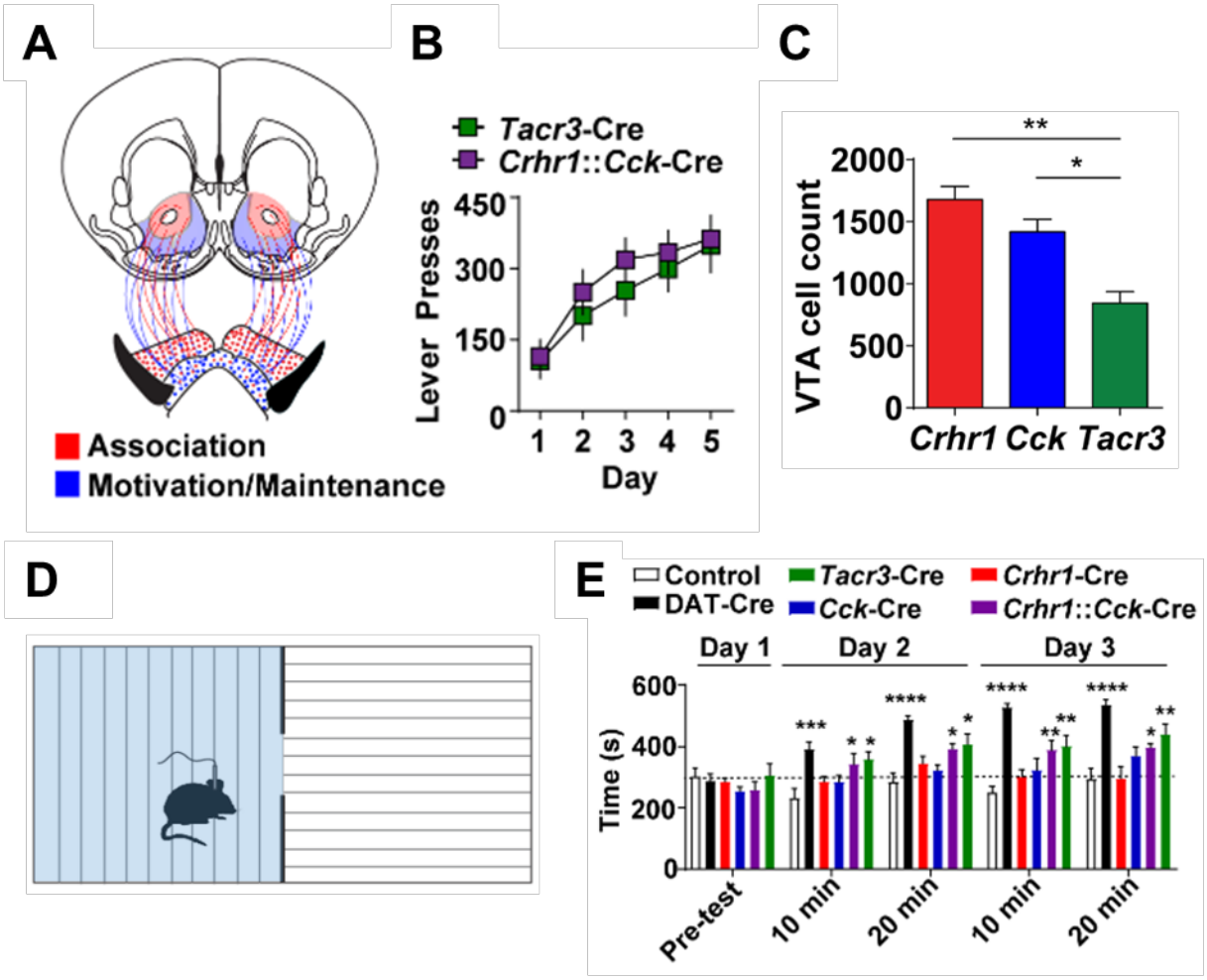

Figure 17. Coordinate actions of associative and motivational VTA neurons for reward reinforcement. (A) Circuit model demonstrating dissociable VTA projections ($Crhr1_{VTA}$, red; Cck_{VTA}, blue) and reward processes. **(B)** Lever presses/day for optogenetic stimulation over 5 FR1 instrumental conditioning days for *Tacr3*-Cre and *Crhr1*-Cre::*Cck*-Cre groups. **(C)** Total cell count of fluorescently labeled neurons identified with AAV1-FLEX-GFP (n=3 mice, 9 sections per animal, *P<0.05, **P<0.01, one-way ANOVA, Bonferroni multiple comparisons). **(D)** Schematic of behavioral apparatus. One side of the two-chamber box was paired with continuous optical stimulation (20 Hz, 5-ms pulse width). **(E)** Real-time place preference (AAV1-FLEX-mCherry control: n=10 mice; DAT-Cre: n=7 mice; *Crhr1*-Cre: n=9 mice; *Cck*-Cre: n=14 mice; *Crhr1*::*Cck*-Cre: n=7 mice; *Tacr3*-Cre: n=6 mice, *P<0.05, **P<0.01, ***P<0.001, ****P<0.0001, two-way ANOVA, Bonferroni selected comparisons to control).

Conclusions and future directions

Here we use a rational genetic approach to segregate VTA dopamine populations for functional interrogation. Through extensive characterization, we establish that neuropeptidergic markers can isolate unique VTA subpopulations and pathways. We identify two populations, *Crhr1*$_{VTA}$ and *Cck*$_{VTA}$ that display differential innervation of mesolimbic targets and response adaptations with extended reward conditioning. Through a combination of optogenetic manipulations and reward behavioral paradigms, we demonstrate that *Crhr1*$_{VTA}$ and *Cck*$_{VTA}$ populations mediate selective, but convergent, reward association and motivation processes.

Mesoaccumbens dopamine-reward pathways

Attempts to delineate functionally-specific dopamine systems have largely focused on distinct output pathways[37,39,40]. Establishing the role of dopamine signaling in the NAc core and shell has been a particularly important, yet challenging endeavor. Projection mapping of genetically-defined VTA subpopulations revealed a striking and complementary segregation of innervation profiles to NAc subregions. In general agreement with the current model of core versus shell dopamine signaling[24,26], we demonstrate that *Crhr1*$_{VTA}$ (core) neurons selectively mediate the formation of response- and stimulus-outcome associations, while *Cck*$_{VTA}$ (shell) neurons motivate or maintain previously learned reward associations. These processes are dissociable and specific

(*Crhr1*$_{VTA}$ neurons are not highly motivating and *Cck*$_{VTA}$ neurons cannot promote associative reward learning), but operate in concert to maximize reinforcement behavior. Co-activation of core and shell projecting dopamine systems, either through *Tacr3*$_{VTA}$ (core and shell) or the double transgenic *Crhr1*::*Cck*, results in rapid acquisition and robust levels of operant responding.

While these subpopulations most densely innervate the NAc, there are also projections to the amygdala. Future studies will need to selectively activate or inhibit distinct circuit components to elucidate the sufficiency and/or necessity of specific VTA-subpopulation output pathways in discrete reward processes. To directly assess if the acquisition of instrumental responding for optogenetic activation of *Crhr1*$_{VTA}$ neurons is dependent on dopamine release in the NAc core, we will repeat the paradigm with pharmacological blockade of dopamine signaling in the NAc. The same approach can be used to probe the requirement of dopamine release in the NAc shell in the motivational function of *Cck*$_{VTA}$ activation. Similarly, dopamine antagonism in the amygdala during these paradigms will help reveal if these pathways work independently or in concert to drive reward behaviors.

Given the opposing innervation patterns in the nucleus accumbens, it is surprising that there is 25% overlap between *Cck*$_{VTA}$ and *Crhr1*$_{VTA}$ subpopulations. Projection analysis of other VTA-receptive brain regions, including the amygdala, suggests that this overlapping population may represent VTA dopamine neuron projections to distinct amygdala subregions and provide an opportunity to isolate additional pathways for functional interrogation. We

have engineered a transgenic *Cck*-Flp mouse to further dissect VTA subpopulations based on genetic phenotype. Double transgenic *Crhr1*-Cre::*Cck*-Flp mice, in combination with Cre- and Flp-dependent viruses will allow for selective characterization and manipulation of this unique population. These double transgenic mice also provide an opportunity to differentially manipulate $Crhr1_{VTA}$ and Cck_{VTA} subpopulations in the same mouse, either simultaneously or in specific epochs of training. For example, Cre-dependent blue-light activated channel rhodopsin can be used to activate the $Crhr1_{VTA}$ subpopulation to promote instrumental learning. Following acquisition, a Flp-dependent red shifted-excitatory opsin (AAV1-frt-Chrimson) can be used to selectively activate Cck_{VTA} neurons to motivate or maintain the learned response. This experiment will strengthen the argument for cooperative interactions between these two subpopulations and pathways. Additionally, it will be interesting to silence one population with tetanus toxin-mediated inhibition of neurotransmitter release or chemogenetic inhibition, while activating the other to assess how each subpopulation can operate without the baseline activity of the other.

Population- and pathway-specific reward encoding

While there is an increasing appreciation for the heterogeneity of dopamine neuron reward encoding[20], how this diversity maps onto distinct output pathways is largely unknown. These divergent projection populations allow unprecedented access to probe circuit-specific reward encoding. Early in training, dopamine neurons exhibit a uniform reward code, displaying similar phasic

activation to reward cues, actions and receipt. Interestingly, we observe an elevation in peri-event baseline activity that coincides with reward pursuit, beginning prior to lever press and persisting through reward receipt. Exploring the functional relevance of this 'tonic ramp' will augment our understanding of how diverse dopamine signals contribute to behavioral outputs. One interesting approach will be to mimic the tonic ramp, either through temporally precise-optogenetic manipulation at lower frequencies, or through a more general chemogenetic strategy. Nuanced manipulation of baseline firing rate during different aspects or periods of reward behavior will likely be necessary to elucidate the specific functional importance. In late conditioning, the tonic ramp is absent in *Crhr1*$_{VTA}$ neurons, but persists in *Cck*$_{VTA}$ neurons. How this differential adaptation relates to reward learning and motivation will be an important point of future investigation.

Peptidergic modulation of the VTA dopamine system

Here we used neuropeptide receptors and the neuropeptide Cck as markers to isolate unique VTA dopamine populations. We did not, however, investigate how peptide signaling within these pathways contributes to behavior. Given the heterogeneity of peptidergic inputs to the VTA, peptidergic modulation of VTA dopamine physiology, and functional specificity of output pathways, it is likely that peptide signaling provides important and behavior-specific modulation of the VTA dopamine system. How Cck and Crh signaling within these pathways contributes to unique functional outputs will be a key component of VTA circuit

study. There are numerous other peptidergic circuits involving the VTA, including orexin/hypocretin[59,60], ghrelin[61,62], oxytocin[63,64] and pituitary adenylate cyclase-activating peptide[65,66] that require further investigation.

Insights for targeted therapeutic approaches

Aberrations in mesolimbic dopamine signaling have been implicated in a variety of neuropsychiatric disorders, including drug addiction and depression[12,13]. To date, current treatment options have limited clinical efficacy and are complicated by significant side effects[67]. The ability to target pathological processes of a specific disease state without impacting adaptive functioning is a necessary step in the effective treatment of dopamine-dependent disorders. Here, we dissociate discrete reward processes of genetically-defined dopamine populations and pathways. Molecular profiling of these populations may uncover selective targets and novel therapeutic approaches[68].

Specifically, the NAc shell has been proposed as the site of altered incentive structure and motivation seen in substance abuse disorders[69-71]. It is possible that *Cck*$_{VTA}$ neurons undergo pathological adaptations in these disorders. *In vivo* and *ex vivo* electrophysiological analysis of these populations before and after drug-related behavioral paradigms will reveal how these neurons change with substance use. Targeted manipulation of these neurons can then be applied in an attempt to prevent pathological adaptations. To translate these findings to clinically useful interventions, gene-expression analysis of *Cck*$_{VTA}$ neurons, in addition to the other dopamine populations, in different phases of

drug use may identify unique molecular targets at discrete interventional stages. Hopefully, this strategy will identify approaches for selective manipulation of isolated populations to attenuate disease processes without altering the wealth of important functions orchestrated by the VTA dopamine system.

This general approach can be further applied to reveal pathologically relevant-dopamine populations in various disease states, as well as to identify specific targets for intervention. Future studies investigating the interaction between specialized dopamine populations and the behavioral domains of mental illness may enhance our understanding and treatment of depression, substance-abuse disorder, ADHD, OCD and schizophrenia.

Experimental Methods

Animals. Male and female mice were housed on a 12-h light/dark cycle. All experiments were performed during the light phase under the guidelines of the Institutional Animal Care and Use Committee at the University of Washington. Mice were aged 2–5 months old for behavioral, 6–8 wk old for electrophysiological and 9–12 wk old for voltammetry experiments.

Generation of Cre-driver mouse lines. *Tacr3-Cre* mice were made by inserting a 4 kb 5' arm and a 4.5 kb 3' arm (each made by PCR amplification from a C57Bl/6 BAC clone with Q5 DNA polymerase and unique restriction sites at each end) into a targeting vector with *ires-Cre:GFP*, frt-flanked *SV-Neo* (for positive selection), *HSV-TK* and *Pgk-DTa* (for negative selection). The targeting construct was electroporated in G4 (129/Sv x C57Bl/6 hybrid) embryonic stem cells. Correct gene targeting was detected in 5 of 77 clones by Southern blot using *EcoR*V and a radioactive probe outside the 5' arm. One of the clones gave high percentage chimeras and germline transmission. The SV-Neo gene was removed by a cross with *Gt(ROSA)26Sor-FLP* recombinase and then *Tacr3-Cre* mice (identified using a 3-primer PCR strategy) were continuously backcrossed to C57Bl/6 mice.

Ntsr1-frtFLEX-Cre mice were made by inserting a 5 kb 5' arm and a 5 kb 3' arm (PCR amplified from a C57Bl/6 BAC clone with Q5 DNA polymerase as above) into a targeting vector with a FLP recombinase-dependent Cre (*ires-frtFLEX-Cre:GFP),* loxP-flanked *SV-Neo* for positive selection and *HSV-TK* and

Pgk-DTa genes for negative selection. A FLP-dependent Cre recombinase was constructed by inserting a *Mt1* gene intron within the open reading frame of mnCre:GFP, which has a Myc tag (m), followed by a nuclear localization signal (NLS, n), followed by Cre recombinase fused to green fluorescent protein (Cre:GFP), to generate a gene with two exons. Then the second exon was inverted and flanked by a pair of dissimilar frt sites to make a double inverted orientation (DIO) construct (denoted as 'FLEX'). The action of FLP recombinase inverts the second exon thereby allowing splicing to generate functional Cre recombinase. The targeting construct was electroporated in G4 (129/Sv x C57Bl/6 hybrid) embryonic stem cells. Correct gene targeting was detected in 11 of 63 clones by Southern blot using *Bgl*II and a radioactive probe outside the 5' arm. One of the clones gave high percentage chimeras and germline transmission. The loxP-flanked SV-Neo gene was removed by a cross with *Meox-Cre* mice. The mice were bred with C57Bl/6 mice to remove the *Meox-Cre* gene and establish C57Bl/6 genetic background. *Ntsr1-Cre* mice were identified using a 3-primer PCR strategy.

Crhr1-FLP-Cre were generated by inserting a 5.9 kb 5' arm and a 4 kb 3' arm (PCR amplified from a C57Bl/6 BAC clone with Q5 DNA polymerase as above) into a targeting vector with a FLP recombinase-dependent Cre (*ires-frtFLEX-Cre:GFP*, as above), loxP-flanked *SV-Neo* for positive selection), with *HSV-TK* and *Pgk-DTa* genes for negative selection. Correct gene targeting was detected in 23 of 42 clones by Southern blot using *EcoR*V and a radioactive probe outside the 5' arm. One of the clones gave high percentage chimeras and

germline transmission. The loxP-flanked SV-Neo gene was removed by a cross with *Meox-Cre* mice. The mice were bred with C57Bl/6 mice to remove the *Meox-Cre* gene and establish C57Bl/6 genetic background. *Ntsr1-FLP-Cre* mice were identified using a 3-primer PCR strategy.

Surgery. Mice were under constant anesthesia (1.5 – 4% isolfurane) and placed in head-fixed stereotax (Model 1900, David Kopf Instruments). Coordinates were standardized to bregma and anterior-posterior positions were adjusted using a correction factor (F = Bregma – Lambda/4.21). The Hamilton injection syringe was lowered 0.5 mm past the indicated depth and 0.5 µl virus was injected at a rate of 0.2 µl/min as the syringe was raised to the desired depth. VTA coordinates (relative to bregma): x = +/-0.5 mm, y = -3.35 mm, z = -4.5 mm.

Mapping Cre-line subpopulations by VTA subregion. A Cre-conditional fluorescent reporter virus (AAV1-FLEX-YFP) was injected bilaterally into the VTA of *Oprk1*-Cre, *Ntsr1*-FLP-Cre, *Tacr3*-Cre, *Crhr1*-Cre or *Cck*-Cre mice. About 3 wks following surgery, 30-µm sections were taken for the rostral-caudal extent of the VTA. One section per atlas image (Paxinos and Franklin, Figures 55-63) was selected and stained overnight with a Rabbit anti-GFP antibody (Invitrogen A11122, 1:2000). Sections were co-stained for tyrosine hydroxylase using a Mouse anti-TH antibody (Millipore MAB318, 1:1000). Images were collected at 10x magnification using a Keyence BZ-X710 fluorescent microscope and

analyzed using ImageJ software. YFP-positive/TH-negative and YFP-positive/TH-positive cells were counted manually

Mapping axon projections from VTA Cre-driver lines. To characterize and quantify the projections of *Oprk1*, *Ntsr1*, *Tacr3*, *Crhr1* or *Cck* populations in the VTA, mice were injected with AAV1-FLEX-synaptophysinGFP bilaterally into the VTA. About 3 wks following surgery, mice were perfused and 30-µm coronal brain sections were collected for the entire brain and stained overnight with a Rabbit anti-GFP antibody (Invitrogen A11122, 1:2000). Every 6^{th} section (every 180 µm) was visually inspected for terminal GFP expression. Images were collected at 10x magnification using a Keyence BZ-X710 fluorescent microscope and analyzed using ImageJ software. After background subtraction, mean pixel intensity was measured. For striatal subregions, mean pixel density was normalized to the mean pixel density at the injection site in the VTA to yield relative density values.

Fast-scan cyclic slice voltammetry. *Crhr1*-Cre, *Cck*-Cre and *Tacr3*-Cre mice (4 - 5 wk old) were injected bilaterally in the VTA with a Cre-conditional Channelrhodopsin virus (AAV1-FLEX-ChR2-mCherry). About 3 wks post-surgery, mice were quickly decapitated and the brain was submerged in ice-cold aCSF solution in which sucrose replaced NaCl. Coronal slices (250 µm) through the striatum were kept in oxygenated aCSF (in mM: 124 NaCl, 2.5 KCl, 1.25 NaH_2PO4, 2 $MgSO_4$, 2 $CaCl_2$, 10 dextrose, and 26 $NaHCO_3$) at 37˚C for an hour

prior to recording. Slices were perfused with oxygenated aCSF at 31-33˚C at 1.5-2.0 mL/min. Dopamine release was recorded with a carbon-fiber microelectrode [72]. The potential at the recording electrode was held at -0.4V vs. an $Ag/AgCl_2$ reference electrode and ramped to +1.3V and back to -0.4V, with one triangular waveform cycle every 100 ms. Waveform generation and data acquisition were performed using software written in LabVIEW (National Instruments, TX). Recordings were performed in three locations per slice: nucleus accumbens medial shell, lateral shell, and core and fluorescence was verified and imaged after recordings. Representative recordings were taken across the A-P axis from +1.5 to +0.7 from bregma. Dopamine release was evoked from ChR2-expressing terminals with a 3-s train (20 Hz, 5-ms pulse width) at 485 nm using the Spectra 4-LCR-XA (Lumencor) light source. Three stimulations were averaged to determine release from each subregion. For each section, measurements were normalized to the largest current amplitude evoked in the slice (from any of the 3 subregions).

Slice Electrophysiology. Horizontal or coronal brain slices (200 or 250 μm, respectively) were prepared in an ice slush solution containing (in mM): 92 NMDG, 2.5 KCl, 1.25 NaH_2PO_4, 30 $NaHCO_3$, 20 HEPES, 25 glucose, 2 thiourea, 5 Na-ascorbate, 3 Na-pyruvate, 0.5 $CaCl_2$, 10 $MgSO_4$, pH 7.3-7.4 [73]. Slices recovered for ≤12 minutes in the same solution at 32°C and then were transferred to a room temperature solution containing (in mM): 92 NaCl, 2.5 KCl, 1.25 NaH_2PO_4, 30 $NaHCO_3$, 20 HEPES, 25 glucose, 2 thiourea, 5 Na-ascorbate,

3 Na-pyruvate, 2 $CaCl_2$, 2 $MgSO_4$. Slices recovered for an additional 45 minutes before recordings were made in aCSF at 32°C continually perfused over slices at a rate of ~2 ml/min and containing (in mM): 126 NaCl, 2.5 KCl, 1.2 NaH2PO4, 1.2 MgCl2 11 D-glucose, 18 NaHCO3, 2.4 CaCl2. All solutions were continually bubbled with O_2/CO_2. Whole-cell recordings were made using an Axopatch 700B amplifier (Molecular Devices) with filtering at 1 kHz using 4-6 MΩ electrodes. A Cre-conditional fluorescent reporter virus (AAV1-FLEX-YFP) was used to identify *Crhr1*, *Cck*, or *Tacr3* neurons for characterization of intrinsic properties. About 3 wk following surgery, 200-µm horizontal brain slices of the VTA were prepared for recording. Electrodes were filled with internal solution containing (in mM): 130 K-Gluconate, 0.1 EGTA, 10 HEPES, 5 Mg-ATP, 0.5 Na-GTP, 5 NaCl, pH 7.3, 280 mOsm. Hyperpolarization-activated (Ih) current was evoked by a hyperpolarizing voltage step from -70 to -120 mV. Tail currents were evoked by repolarization to -60 mV following a 500-ms voltage step to 0 mV from a holding potential of -60 mV. The amplitude was calculated from the average of 5 sweeps. Baseline firing rate was recorded in current clamp mode. For a subset of cells with stable firing, quinpirole (1 mM) was washed into the bath to assess D2 sensitivity. Resting membrane potential was also measured during current-clamp recordings. For light-evoked EPSC and IPSC recordings of VTA outputs to nucleus accumbens subregions, *Crhr1*-Cre, *Cck*-Cre and *Tacr3*-Cre mice (4 – 5 wk old) were injected bilaterally in the VTA with a Cre-conditional Channelrhodopsin virus (AAV1-FLEX-ChR2-mCherry). About 3 wks post-surgery, 250-µm coronal brain slices of the striatum were prepared for recording.

Electrodes were filled with internal solution containing (in mM): 132 $CsMeSO_3$, 8 CsCl, 10 HEPES, 1 EGTA, 0.5 $CaCl_2$, 10 Glucose, 5 QX-314, pH 7.3, 280 mOsm. Light-evoked synaptic transmission was induced with 5-ms light pulses delivered at 0.1 Hz from an optic fiber placed directly in the bath. Light-evoked EPSCs were recorded while holding at -60 mV and IPSCs were recorded while holding at 0 mV. CNQX (10 μM) was applied to the bath solution to block excitatory and feed-forward inhibition responses. Picrotoxin (100 μM) was applied to block IPSCs. Amplitudes and example current traces represent an average of at least 10 events.

RNAscope in situ hybridization. The RNAscope assay (acdBio) was performed on Bl6 wild-type adult mice[74]. Briefly, brains were quickly excised, flash frozen in 2-methylbutane, and stored at -80 degrees Celsius. 10-μm brain slices were prepared for the rostral, medial and caudal VTA for each animal. Sections were prepared for hybridization per manufacturer's instructions using probes for *Crhr1* (Mm-*Crhr1*) and *Cck* (Mm-*Cck*-C3; 1:50 dilution). Slides were cover slipped and imaged using a Keyence BZ-X710 fluorescent microscope. Overlap was quantified for each section at 10x magnification using ImageJ software.

In vivo electrophysiology A microdrive containing an optic fiber and four recording tetrodes (25-μm diameter tungsten wire; California Fine Wire) was implanted dorsal to the VTA (3.7 mm to the brain surface) after AAV-FLEX-ChR2-mCherry was infused[75]. The distance between the fiber and tetrode tips

was kept less than 500 μm. After recovery, each mouse was food-restricted to 85% and shaped to press a lever for a food pellet in an operant box for 2 days. After the habituation, the mouse was placed in a holding cage and single-unit activity was monitored using a Cheetah data acquisition system (Digital Lynx 4SX, Neuralynx). To identify ChR2-expressing neurons in the VTA, 10 blue-light pulses (473 nm; 5-ms long at 20 Hz; Laserglow technologies) were presented via the optic fiber of the microdrive. The light intensity (5–15 mW/mm^2) was adjusted so that light-evoked spike waveforms were similar to spontaneous ones. Once some light-responsive units were found, the mouse underwent 10 daily recording sessions. In each session, neuronal responses to the light pulses were first recorded in the holding cage. Then basal firing patterns were measured in the operant box for 10 min. Then the behavioral recording was conducted for 1 hour. After the recording session, all tetrodes were lowered in 80-μm increments to find different light-responsive units. If no light-responsive units were observed on a given day, the tetrodes were moved down until new light-responsive units were encountered. These neuronal responses during the operant conditioning were recorded on the following day.

To analyze the unit data, single units were isolated based on various waveform features using an Offline Sorter (Plexon). Only units showing good recording stability throughout the whole recording session were included for further analysis. To categorize light-responsive neurons, a cluster analysis was performed based on spike probability and spike latency in response to blue light pulses. The cluster that has high probability (>0.63) and short latency (<9.9 ms)

was considered as light-responsive neurons. The cluster also showed high correlations between spontaneous and light-evoked waveforms. These neuronal responses to the cue, action, and reward during the operant conditioning were examined with peri-event time histograms (PETHs; 50-ms bins) constructed around the times of the three events. Firing rates in PETHs were transformed to z-scores relative to basal firing rates during the 10-min recording period prior to the operant conditioning. A VTA cells was classified as responsive to each event if its average z-score during each event period (cue, 0 to 300 ms; action, -100 to 200 ms; reward, -50 to 350 ms) was greater than 2.5.

Optogenetic excitation/inhibition and reinforcement-conditioning paradigms. For activation of VTA subpopulations, AAV1-FLEX-ChR2-mCherry was injected unilaterally into the VTA of adult mice. A custom-built, optic fiber was implanted 0.5 mm dorsal to the injection site and affixed to the skull with Metabond and dental cement. Only optic fibers with > 70% power retention were used. For all experiments (except real-time place preference), mice were maintained at 85 – 90 % of baseline body weight starting 1 wk prior to experimentation. All operant and Pavlovian conditioning assays were performed in Med Associates Inc. behavior boxes. Each behavior box had 2 levers positioned on either side of a food hopper on one wall, with a house light centered on the opposite wall. A 20-mg sugar pellet was the natural food reward. Animals received a 3-s, 20-Hz stimulation train with 5-ms pulses for optogenetic activation. Power output was adjusted to ~10 mW at the tip of the optic fiber

under constant illumination. For all experiments, control mice were injected with AAV1-FLEX-mCherry.

Primary reinforcement for optical stimulation

Naïve animals were placed in the operant conditioning boxes for 1-hour sessions for 5 consecutive days. At baseline, both levers were extended and the house light was illuminated. Each lever press (FR1, either lever) resulted in lever retraction, the house light turning off and a 3-s train of optical stimulation at 20 Hz for 5 s following lever press/retraction, the levers re-extended and the house light was re-illuminated.

Primary reinforcement for food reward followed by optical stimulation

Naïve animals were placed in the operant conditioning boxes for 1-h sessions for 10 consecutive days. At baseline, both levers were extended and the house light was illuminated. For the first 5 days of training, each lever press (FR1, either lever) resulted in immediate delivery of a 20-mg food pellet into the food hopper, in addition to lever retraction and the house light turning off. To promote learning of the contingency, the levers remained retracted and the house light off until a head entry into the food hopper was made. For training days 6 – 10, food pellet reward was exchanged for optical stimulation as above (FR1, either lever).

Primary reinforcement for food reward vs. optical stimulation

Animals underwent 3 days of instrumental conditioning for food pellet reward identical to the 1st 5 days of training above. Right and left lever presses were recorded. On the 4th day of training, one of the two levers was assigned to result in optical stimulation, while the other continued to result in food reward. This was

counterbalanced to give equal lever presses on ‘food-paired’ and ‘light-paired’ levers prior to the transition on training day 4.

Progressive ratio

Animals that had previously learned to lever press for optical stimulation underwent an additional day of testing where the number of presses required to deliver optical stimulation increased non-arithmetically (i.e. 1, 2, 4, 6, 9, 13…) over the course of the session. The session ended after 3 consecutive minutes of no lever presses. Break point indicates the number of lever presses in the last successfully completed ratio.

Pavlovian conditioning and instrumental transfer

Mice were bilaterally injected in the VTA with the red-shifted inhibitory opsin Jaws (AAV1-FLEX-Jaws-GFP). Bilateral cannulas were implanted 0.5 mm dorsal to the injection sites; one was lowered straight down while the other was implanted at a 10-degree angle. Optical inhibition for 3 s was delivered bilaterally through a split patch cable adjusted to give ~10 mW power at each optic fiber tip under constant illumination. Training sessions consisted of 25 trials in which 10-s lever extension (CS) was immediately followed by food pellet reward (US). Each trial was separated by a random inter-trial interval averaging 70 s and animals underwent 8 days of training. Optical inhibition for 3 s began 100 ms prior to CS onset. A pulse (2 s), ramp-down (1 s) laser sequence was used to limit rebound excitation after laser-off. Head entries were recorded and quantified as a-per minute metric. After the 8 days of Pavlovian conditioning, mice were tested on an FR1 (food

reward, either lever) task identical to primary reinforcement for food reward as above for 3 additional days.

Real-time place preference.

A custom made 2-chamber box was constructed with each chamber having unique contextual cues (horizontal vs. vertical wall stripes). An opening allowed free movement between the 2 chambers. On pre-test day 1, animals were attached to the patch cord and placed in the box for 10 min without any optical stimulation. On subsequent days, the light-paired side was counterbalanced to account for any preference. On test days 2 and 3, the light-paired side was paired with continuous optical excitation (ChR2: 20 Hz, 5-ms pulse width) or inhibition (Jaws: 2-s pulse, 1-s ramp down, 1 s off) for the 20-min session. Post-test day 4 was done without stimulation for 10 min.

Statistical Analysis. Data were analyzed using GraphPad Prism version 6. For comparison of multiple treatments, a repeated measures one-way ANOVA with Tukey's post hoc multiple comparisons test between all groups was used (unless stated otherwise in the text). For analysis of experiments with multiple treatments and time-points, a two-way repeated measures ANOVA with Sidak's post hoc multiple comparisons test was used. Multiple comparisons correspond to time-points unless otherwise stated. Two-tailed student's t-test were used. All data are represented as mean +/- S.E.M..

References

1 Berridge, K. C. The debate over dopamine's role in reward: the case for incentive salience. *Psychopharmacology (Berl)* **191**, 391-431, doi:10.1007/s00213-006-0578-x (2007).

2 Schultz, W., Dayan, P. & Montague, P. R. A neural substrate of prediction and reward. *Science* **275**, 1593-1599 (1997).

3 Salamone, J. D. & Correa, M. The mysterious motivational functions of mesolimbic dopamine. *Neuron* **76**, 470-485, doi:10.1016/j.neuron.2012.10.021 (2012).

4 Goto, Y. & Grace, A. A. Dopaminergic modulation of limbic and cortical drive of nucleus accumbens in goal-directed behavior. *Nat Neurosci* **8**, 805-812, doi:10.1038/nn1471 (2005).

5 Goto, Y. & Grace, A. A. Dopamine modulation of hippocampal-prefrontal cortical interaction drives memory-guided behavior. *Cereb Cortex* **18**, 1407-1414, doi:10.1093/cercor/bhm172 (2008).

6 Horvitz, J. C. Stimulus-response and response-outcome learning mechanisms in the striatum. *Behav Brain Res* **199**, 129-140, doi:10.1016/j.bbr.2008.12.014 (2009).

7 O'Donnell, P. & Grace, A. A. Synaptic interactions among excitatory afferents to nucleus accumbens neurons: hippocampal gating of prefrontal cortical input. *J Neurosci* **15**, 3622-3639 (1995).

8 Flagel, S. B. *et al.* A selective role for dopamine in stimulus-reward learning. *Nature* **469**, 53-57, doi:10.1038/nature09588 (2011).

9 Hart, A. S., Clark, J. J. & Phillips, P. E. M. Dynamic shaping of dopamine signals during probabilistic Pavlovian conditioning. *Neurobiol Learn Mem* **117**, 84-92, doi:10.1016/j.nlm.2014.07.010 (2015).

10 Berridge, K. C. & Robinson, T. E. What is the role of dopamine in reward: hedonic impact, reward learning, or incentive salience? *Brain Res Brain Res Rev* **28**, 309-369 (1998).

11 Saunders, B. T. & Robinson, T. E. The role of dopamine in the accumbens core in the expression of Pavlovian-conditioned responses. *Eur J Neurosci* **36**, 2521-2532, doi:10.1111/j.1460-9568.2012.08217.x (2012).

12 Dunlop, B. W. & Nemeroff, C. B. The role of dopamine in the pathophysiology of depression. *Arch Gen Psychiatry* **64**, 327-337, doi:10.1001/archpsyc.64.3.327 (2007).

13 Volkow, N. D., Fowler, J. S., Wang, G. J. & Swanson, J. M. Dopamine in drug abuse and addiction: results from imaging studies and treatment implications. *Mol Psychiatry* **9**, 557-569, doi:10.1038/sj.mp.4001507 (2004).

14 Robinson, T. E. & Berridge, K. C. The neural basis of drug craving: an incentive-sensitization theory of addiction. *Brain Res Brain Res Rev* **18**, 247-291 (1993).

15 Robinson, T. E. & Berridge, K. C. Incentive-sensitization and addiction. *Addiction* **96**, 103-114, doi:10.1080/09652140020016996 (2001).

16 Carlsson, A. Thirty years of dopamine research. *Adv Neurol* **60**, 1-10 (1993).

17 Sesack, S. R. & Grace, A. A. Cortico-Basal Ganglia reward network: microcircuitry. *Neuropsychopharmacology* **35**, 27-47, doi:10.1038/npp.2009.93 (2010).
18 Swerdlow, N. R., Braff, D. L., Masten, V. L. & Geyer, M. A. Schizophrenic-like sensorimotor gating abnormalities in rats following dopamine infusion into the nucleus accumbens. *Psychopharmacology (Berl)* **101**, 414-420 (1990).
19 Swerdlow, N. R. *et al.* Amphetamine disruption of prepulse inhibition of acoustic startle is reversed by depletion of mesolimbic dopamine. *Psychopharmacology (Berl)* **100**, 413-416 (1990).
20 Bromberg-Martin, E. S., Matsumoto, M. & Hikosaka, O. Dopamine in motivational control: rewarding, aversive, and alerting. *Neuron* **68**, 815-834, doi:10.1016/j.neuron.2010.11.022 (2010).
21 Niv, Y., Daw, N. D., Joel, D. & Dayan, P. Tonic dopamine: opportunity costs and the control of response vigor. *Psychopharmacology (Berl)* **191**, 507-520, doi:10.1007/s00213-006-0502-4 (2007).
22 Howe, M. W., Tierney, P. L., Sandberg, S. G., Phillips, P. E. & Graybiel, A. M. Prolonged dopamine signalling in striatum signals proximity and value of distant rewards. *Nature* **500**, 575-579, doi:10.1038/nature12475 (2013).
23 Bromberg-Martin, E. S., Matsumoto, M. & Hikosaka, O. Distinct Tonic and Phasic Anticipatory Activity in Lateral Habenula and Dopamine Neurons. *Neuron* **67**, 144-155, doi:10.1016/j.neuron.2010.06.016 (2010).
24 Floresco, S. B. The nucleus accumbens: an interface between cognition, emotion, and action. *Annu Rev Psychol* **66**, 25-52, doi:10.1146/annurev-psych-010213-115159 (2015).
25 Saddoris, M. P., Cacciapaglia, F., Wightman, R. M. & Carelli, R. M. Differential Dopamine Release Dynamics in the Nucleus Accumbens Core and Shell Reveal Complementary Signals for Error Prediction and Incentive Motivation. *J Neurosci* **35**, 11572-11582, doi:10.1523/JNEUROSCI.2344-15.2015 (2015).
26 Saddoris, M. P., Sugam, J. A., Cacciapaglia, F. & Carelli, R. M. Rapid dopamine dynamics in the accumbens core and shell: learning and action. *Front Biosci (Elite Ed)* **5**, 273-288 (2013).
27 Hart, A. S., Rutledge, R. B., Glimcher, P. W. & Phillips, P. E. Phasic dopamine release in the rat nucleus accumbens symmetrically encodes a reward prediction error term. *J Neurosci* **34**, 698-704, doi:10.1523/JNEUROSCI.2489-13.2014 (2014).
28 Beyeler, A. *et al.* Divergent Routing of Positive and Negative Information from the Amygdala during Memory Retrieval. *Neuron* **90**, 348-361, doi:10.1016/j.neuron.2016.03.004 (2016).
29 Otis, J. M. *et al.* Prefrontal cortex output circuits guide reward seeking through divergent cue encoding. *Nature* **543**, 103-107, doi:10.1038/nature21376 (2017).
30 Morales, M. & Margolis, E. B. Ventral tegmental area: cellular heterogeneity, connectivity and behaviour. *Nat Rev Neurosci* **18**, 73-85, doi:10.1038/nrn.2016.165 (2017).
31 Stuber, G. D., Hnasko, T. S., Britt, J. P., Edwards, R. H. & Bonci, A. Dopaminergic terminals in the nucleus accumbens but not the dorsal striatum corelease

glutamate. *J Neurosci* **30**, 8229-8233, doi:10.1523/JNEUROSCI.1754-10.2010 (2010).
32 Tritsch, N. X., Ding, J. B. & Sabatini, B. L. Dopaminergic neurons inhibit striatal output through non-canonical release of GABA. *Nature* **490**, 262-266, doi:10.1038/nature11466 (2012).
33 Brown, M. T. *et al.* Ventral tegmental area GABA projections pause accumbal cholinergic interneurons to enhance associative learning. *Nature* **492**, 452-456, doi:10.1038/nature11657 (2012).
34 van Zessen, R., Phillips, J. L., Budygin, E. A. & Stuber, G. D. Activation of VTA GABA neurons disrupts reward consumption. *Neuron* **73**, 1184-1194, doi:10.1016/j.neuron.2012.02.016 (2012).
35 Tan, K. R. *et al.* GABA neurons of the VTA drive conditioned place aversion. *Neuron* **73**, 1173-1183, doi:10.1016/j.neuron.2012.02.015 (2012).
36 Yoo, J. H. *et al.* Ventral tegmental area glutamate neurons co-release GABA and promote positive reinforcement. *Nat Commun* **7**, 13697, doi:10.1038/ncomms13697 (2016).
37 Beier, K. T. *et al.* Circuit Architecture of VTA Dopamine Neurons Revealed by Systematic Input-Output Mapping. *Cell* **162**, 622-634, doi:10.1016/j.cell.2015.07.015 (2015).
38 Lammel, S. *et al.* Unique properties of mesoprefrontal neurons within a dual mesocorticolimbic dopamine system. *Neuron* **57**, 760-773, doi:10.1016/j.neuron.2008.01.022 (2008).
39 Lammel, S., Lim, B. K. & Malenka, R. C. Reward and aversion in a heterogeneous midbrain dopamine system. *Neuropharmacology* **76 Pt B**, 351-359, doi:10.1016/j.neuropharm.2013.03.019 (2014).
40 Lammel, S. *et al.* Input-specific control of reward and aversion in the ventral tegmental area. *Nature* **491**, 212-217, doi:10.1038/nature11527 (2012).
41 Sanz, E. *et al.* Cell-type-specific isolation of ribosome-associated mRNA from complex tissues. *Proc Natl Acad Sci U S A* **106**, 13939-13944, doi:10.1073/pnas.0907143106 (2009).
42 Chung, A. S., Miller, S. M., Sun, Y., Xu, X. & Zweifel, L. S. Sexual congruency in the connectome and translatome of VTA dopamine neurons. *Sci Rep* **7**, 11120, doi:10.1038/s41598-017-11478-5 (2017).
43 Borgland, S. L., Ungless, M. A. & Bonci, A. Convergent actions of orexin/hypocretin and CRF on dopamine neurons: Emerging players in addiction. *Brain Res* **1314**, 139-144, doi:10.1016/j.brainres.2009.10.068 (2010).
44 Kalivas, P. W. Interactions between neuropeptides and dopamine neurons in the ventromedial mesencephalon. *Neurosci Biobehav Rev* **9**, 573-587 (1985).
45 Tyree, S. M. & de Lecea, L. Lateral Hypothalamic Control of the Ventral Tegmental Area: Reward Evaluation and the Driving of Motivated Behavior. *Front Syst Neurosci* **11**, 50, doi:10.3389/fnsys.2017.00050 (2017).
46 Werkman, T. R., McCreary, A. C., Kruse, C. G. & Wadman, W. J. NK3 receptors mediate an increase in firing rate of midbrain dopamine neurons of the rat and the guinea pig. *Synapse* **65**, 814-826, doi:10.1002/syn.20908 (2011).

47 Lemos, J. C. *et al.* Severe stress switches CRF action in the nucleus accumbens from appetitive to aversive. *Nature* **490**, 402-406, doi:10.1038/nature11436 (2012).
48 Wanat, M. J., Bonci, A. & Phillips, P. E. CRF acts in the midbrain to attenuate accumbens dopamine release to rewards but not their predictors. *Nat Neurosci* **16**, 383-385, doi:10.1038/nn.3335 (2013).
49 Wanat, M. J., Hopf, F. W., Stuber, G. D., Phillips, P. E. & Bonci, A. Corticotropin-releasing factor increases mouse ventral tegmental area dopamine neuron firing through a protein kinase C-dependent enhancement of Ih. *J Physiol* **586**, 2157-2170, doi:10.1113/jphysiol.2007.150078 (2008).
50 Walsh, J. J. *et al.* Stress and CRF gate neural activation of BDNF in the mesolimbic reward pathway. *Nat Neurosci* **17**, 27-29, doi:10.1038/nn.3591 (2014).
51 Lima, S. Q., Hromadka, T., Znamenskiy, P. & Zador, A. M. PINP: a new method of tagging neuronal populations for identification during in vivo electrophysiological recording. *PLoS One* **4**, e6099, doi:10.1371/journal.pone.0006099 (2009).
52 Witten, I. B. *et al.* Recombinase-driver rat lines: tools, techniques, and optogenetic application to dopamine-mediated reinforcement. *Neuron* **72**, 721-733, doi:10.1016/j.neuron.2011.10.028 (2011).
53 Tsai, H. C. *et al.* Phasic firing in dopaminergic neurons is sufficient for behavioral conditioning. *Science* **324**, 1080-1084, doi:10.1126/science.1168878 (2009).
54 Hodos, W. Progressive Ration as a Measure of Reward Strength. *Science* **134**, 943-&, doi:DOI 10.1126/science.134.3483.943 (1961).
55 Darvas, M., Henschen, C. W. & Palmiter, R. D. Contributions of signaling by dopamine neurons in dorsal striatum to cognitive behaviors corresponding to those observed in Parkinson's disease. *Neurobiology of disease* **65**, 112-123, doi:10.1016/j.nbd.2014.01.017 (2014).
56 Lein, E. S. *et al.* Genome-wide atlas of gene expression in the adult mouse brain. *Nature* **445**, 168-176, doi:10.1038/nature05453 (2007).
57 Bolam, J. P. & Smith, Y. The GABA and substance P input to dopaminergic neurones in the substantia nigra of the rat. *Brain research* **529**, 57-78 (1990).
58 Valentino, R. J., Reyes, B., Van Bockstaele, E. & Bangasser, D. Molecular and cellular sex differences at the intersection of stress and arousal. *Neuropharmacology* **62**, 13-20, doi:10.1016/j.neuropharm.2011.06.004 (2012).
59 Korotkova, T. M., Sergeeva, O. A., Eriksson, K. S., Haas, H. L. & Brown, R. E. Excitation of ventral tegmental area dopaminergic and nondopaminergic neurons by orexins/hypocretins. *J Neurosci* **23**, 7-11 (2003).
60 Moorman, D. E. & Aston-Jones, G. Orexin/hypocretin modulates response of ventral tegmental dopamine neurons to prefrontal activation: diurnal influences. *J Neurosci* **30**, 15585-15599, doi:10.1523/JNEUROSCI.2871-10.2010 (2010).

61 Abizaid, A. Ghrelin and dopamine: new insights on the peripheral regulation of appetite. *J Neuroendocrinol* **21**, 787-793, doi:10.1111/j.1365-2826.2009.01896.x (2009).

62 Abizaid, A. *et al.* Ghrelin modulates the activity and synaptic input organization of midbrain dopamine neurons while promoting appetite. *J Clin Invest* **116**, 3229-3239, doi:10.1172/JCI29867 (2006).

63 Baskerville, T. A. & Douglas, A. J. Dopamine and oxytocin interactions underlying behaviors: potential contributions to behavioral disorders. *CNS Neurosci Ther* **16**, e92-123, doi:10.1111/j.1755-5949.2010.00154.x (2010).

64 Hung, L. W. *et al.* Gating of social reward by oxytocin in the ventral tegmental area. *Science* **357**, 1406-1411, doi:10.1126/science.aan4994 (2017).

65 Marquez, P. *et al.* The role of endogenous PACAP in motor stimulation and conditioned place preference induced by morphine in mice. *Psychopharmacology (Berl)* **204**, 457-463, doi:10.1007/s00213-009-1476-9 (2009).

66 Masuo, Y. *et al.* Autoradiographic distribution of pituitary adenylate cyclase activating polypeptide (PACAP) binding sites in the rat brain. *Neurosci Lett* **126**, 103-106 (1991).

67 Ferguson, J. M. SSRI Antidepressant Medications: Adverse Effects and Tolerability. *Prim Care Companion J Clin Psychiatry* **3**, 22-27 (2001).

68 Greene, J. G. Gene expression profiles of brain dopamine neurons and relevance to neuropsychiatric disease. *J Physiol* **575**, 411-416, doi:10.1113/jphysiol.2006.112599 (2006).

69 Di Chiara, G. Nucleus accumbens shell and core dopamine: differential role in behavior and addiction. *Behav Brain Res* **137**, 75-114 (2002).

70 Di Chiara, G. *et al.* Dopamine and drug addiction: the nucleus accumbens shell connection. *Neuropharmacology* **47 Suppl 1**, 227-241, doi:10.1016/j.neuropharm.2004.06.032 (2004).

71 Di Chiara, G. *et al.* Drug addiction as a disorder of associative learning. Role of nucleus accumbens shell/extended amygdala dopamine. *Ann N Y Acad Sci* **877**, 461-485 (1999).

72 Clark, J. J. *et al.* Chronic microsensors for longitudinal, subsecond dopamine detection in behaving animals. *Nature methods* **7**, 126-129, doi:10.1038/nmeth.1412 (2010).

73 Ting, J. T., Daigle, T. L., Chen, Q. & Feng, G. Acute brain slice methods for adult and aging animals: application of targeted patch clamp analysis and optogenetics. *Methods Mol Biol* **1183**, 221-242, doi:10.1007/978-1-4939-1096-0_14 (2014).

74 Wang, F. *et al.* RNAscope: a novel in situ RNA analysis platform for formalin-fixed, paraffin-embedded tissues. *J Mol Diagn* **14**, 22-29, doi:10.1016/j.jmoldx.2011.08.002 (2012).

75 Gore, B. B. *et al.* Roundabout receptor 2 maintains inhibitory control of the adult midbrain. *Elife* **6**, doi:10.7554/eLife.23858 (2017).